INFRARED OBSERVATION OF THE GALATIC CENTER

Thesis by

Eric Edward Becklin

In Partial Fulfillment of the Requirements

For the Degree of

Doctor of Philosophy

California Institute of Technology

Pasadena, California

1968

(Submitted May 13, 1968)

ACKNOWLEDGMENTS

It is a pleasure to thank my research advisor, Dr. G. Neugebauer, for his continued aid and advice. In particular, I am greatly indebted for his assistance in preparing and writing the paper, Infrared Observations of the Galactic Center, Becklin, E. E., Neugebauer, G., 1968, Ap. J., 151, 145, upon which most of this thesis is based.

I would also like to thank all others connected with the infrared sky survey at the California Institute of Technology for their assistance. I would especially like to thank G. Neugebauer, T. Hilgeman, D. Martz, D. McCammon and P. Trapane for help in building and testing the infrared equipment.

For assisting in the telescope observations I thank G. Neugebauer and A. McKay, as well as, V. Hett, T. Hilgeman, R. Jacques, C. Kearns, H. Schaefer, G. Tuton and J. Westphal.

For valuable discussions I wish to thank Mr. E. Hughes and Drs. J. L. Greenstein, R. B. Leighton, G. Münch, M. Schmidt and I. S. Shklovskii.

For use of the telescopes I thank Dr. H. W. Babcock of the Mount Wilson and Palomar Observatories.

ABSTRACT

Infrared radiation from the nucleus of the galaxy has been detected at effective wavelengths of 1.65, 2.2, 3.4 and 4.8 μ with angular resolutions from 0.04 to 1.8 arc min. Observations have been made over an area of 1 square degree surrounding the dynamical center of the Galaxy.

The reduced data consist of contour maps of the 2.2 μ brightness distribution of the galactic center region for resolutions of 1.8, 0.8, and 0.25 arc min, and of tabulations of the 1.65, 2.2, 3.4, and 4.8 μ flux densities and surface brightnesses at various areas in the galactic center region.

From the brightness distribution maps it is found that the structure consists of: (1) a dominant source 5 arc min in diameter, (2) a point-like source centered on the dominant source, (3) an extended background approximately 1 degree in diameter, (4) additional discrete extended sources which are fainter than the dominant source.

A comparison of the infrared and radio observations shows that the dominant infrared source and the radio source Sagittarius A have the same coordinates and similar sizes.

An analysis of the observed infrared radiation predicts about 25 magnitudes of visual absorption between the Sun and the galactic center if the source of infrared radiation is stellar. A comparison is also made between the infrared radiation from the galactic center and that from the nucleus of M 31 which shows agreement in both the apparent structure and infrared luminosity of the two nuclei.

TABLE OF CONTENTS

INTRODUCTION

In the 40 years which have elapsed since Hubble discovered that spiral nebulae are extragalactic in nature and that they probably are similar to the Milky Way, many observations have been made which have increased our knowledge of galactic structure. These observations show that spiral nebulae and the Galaxy can be divided into three parts: a) a flat disk, 5 - 20 kpc in diameter and about 1 kpc thick, which shows much spiral structure and contains young bright stars, gas, and dust; b) a faint spherical halo surrounding the disk which contains very old stars; and c) a bright spherical nuclear bulge a few kiloparsecs in diameter at the center of the disk. The observations presented in this paper are concerned with the very central region of the galactic nuclear bulge; specifically the results of the first observations of the central 200 pc of the Galaxy at wavelengths near the visual region are given.

Some general properties of the nuclear bulge of spiral galaxies have been determined from observations of extragalactic nebulae. These observations show a large range in the linear size and luminosity of the nuclear region. The surface brightness and mass density is generally much higher in the nuclear bulge than in the disk (31). The luminosity appears to originate from late population I like stars; the spectral energy distribution and the absorption line features are similar to G, K and M stars (32). From observations of the nearby spiral galaxy M 31 it has been shown that the surface brightness and mass density increase rapidly as the distance to the center of the nucleus decreases. At the

very center there is a bright star-like region with a diameter less than 10 pc (8, 9). Rotational velocity studies of this 10 pc region (10) in M 31 show a mass density 10^4 times larger than the density in the solar neighborhood.

In the Galaxy the dynamical center lies 10 kpc from the Sun in the direction of the constellation Sagittarius (1, 2). Most of the details about the galactic center have been obtained through observations at radio wavelengths; however, some limited observations at optical wavelengths have been made.

Because of the obscuration by interstellar dust, visual and near infrared observations in the past have been limited to regions at the edge of the nuclear bulge. Several observations (4, 5, 6, 7) have been made of regions about 1 kpc from the dynamical center. The results of these observations show that the bulge of the Galaxy has a population similar to nuclei of external galaxies. The bulge appears to be smaller and fainter than the nuclear region of M 31.

Radio observations of the galactic center can be discussed in two parts, 1) 21 cm hydrogen line studies of the motions of gas, and 2) continuum studies of sources present in the nucleus. A summary of the 21 cm observations is given by Rougoor and Oort (25). These observations have shown that within a 200 pc diameter sphere a mass of 10^9 $M_\odot$ exists. The observations also have been used to determine the dynamical center of the Galaxy to an accuracy of 5 arc min (1). Continuum studies of the galactic center region have recently been summarized by Downes and Maxwell (3). The continuum radio radiation from the central region of the galactic nucleus ($\sim$ 200 pc diameter) can

be divided into three parts: a) a strong non-thermal source Sagittarius A 10 pc in diameter, b) several thermal sources (H II regions) fainter than Sagittarius A, and c) an extended background one degree (180 pc) in diameter. The 10 pc source Sagittarius A is coincident with the dynamical center of the Galaxy.

In summary we see that the very central regions of some external spiral nebulae have a small bright optical core about 10 pc in size. In the Galaxy, radio observations indicate the presence of a 10 pc non-thermal source at the galactic center. It is clear that to have a better understanding of the nature of the center of the Galaxy as well as galactic nuclei in general, it is important to have direct observations of the galactic center at visual wavelengths. However, as stated above these observations are impossible because of the large amount of absorption by interstellar dust. On the other hand, it is well-known that the amount of obscuration decreases at infrared wavelengths. Because of this apparent transparency in the infrared, several attempts have been made to observe a small nucleus in the Galaxy. The results of three of these observations have been published.

In 1945, Stebbins and Whitford (4), using a photocell at an effective wavelength of 1.03 μ, scanned across the galactic equator in a region thought to be close to the galactic center. With an 8.6 arc min diameter aperture they scanned an area of approximately 50 square degrees centered on the 1950 coordinate RA = $17^h\ 35^m$ Dec = -29.5°. Although they scanned across the position of the dynamical center they detected no radiation from a possible source in that direction. They

did detect infrared radiation 2 to 3 degrees west of the dynamical center which indicated the presence of the nuclear bulge discussed above.

In the early 1950's Baade (8) attempted to find a 10 pc nucleus in the Galaxy. Using the most sensitive infrared plates known, he photographed the region around the radio source Sagittarius A, but was unable to detect any extended source of radiation.

In 1960 Moroz (11) made scans across the galactic equator in the vicinity of Sagittarius A at an effective wavelength of 1.7 μ. Using a PbS detector and a 1.7 arc min aperture he made six right ascension scans, 20 arc min long, in a region centered on the 1950 position RA = 17^h 42.5^m Dec = - 28° 56'. With a limiting 1.7 μ magnitude of about 6.5 he was unable to detect any radiation, and therefore concluded that one or more of the following statements must be correct:

a) The galactic nucleus is a factor of 10 fainter than the 10 pc core in M 31.

b) Almost 30 magnitudes of photographic absorption is present between the Sun and the galactic center.

c) The standard interstellar absorption law of Whitford (12) is incorrect.

d) The galactic center lies outside the region scanned.

During the summer of 1966, after discussing the problem with a fellow graduate student, E. Hughes, it was decided that an attempt should be made to observe the galactic nucleus with our infrared photometer. The two main reasons for making this decision were: a) the photometer was optimized to detect radiation in the 2.0 to 2.4 μ region, while according to Whitfords (12) absorption law and the wavelength

sensitivity of infrared detectors, 2 to 3 μ was the best wavelength region to make the observations, and b) the photometer had a maximum field of view of 1.8 arc min (5 pc at the galactic center) when mounted on the 24-inch telescope, which was approximately the same size as the central nucleus in M 31 and Sagittarius A.

In August 1966, with the help of a student, Andrew McKay, the region around Sagittarius A was scanned on the 24-inch telescope. With a limiting 2.2 μ magnitude of about 5, infrared radiation was discovered with a signal to noise ratio of about 10:1. Subsequent to this discovery, a region 30 arc min in diameter (100 pc) was mapped at 2.2 μ on the 24-inch. Mapping was also done on the 60- and 200-inch telescopes with finer resolutions. Further photometric measurements were made at the wavelengths around 1.65, 3.4, and 4.8 μ, although the 4.8 μ measurements were made in a very limited region and were of a poor quality.

II. INSTRUMENTATION

A. Photometer

The observations were made using an infrared photometer mounted on optical telescopes. The photometer, shown schematically in Fig. 1, has a mirrored 5 Hz chopper which alternatively admits radiation from the field to be measured and from an out of focus reference field 5 cm away. A reference field in the sky is normally used to cancel fluctuations in the background emission from the telescope and atmosphere, but under special conditions a constant temperature black body reference can be substituted. To view the signal field visually, a 45° mirror is inserted across the beam, diverting the radiation to an eye piece.

Three different detector systems can be mounted on the photometer at one time. Two of the systems are mounted on a movable slide on the top of the photometer (PbS detector in Fig. 1). The slide is keyed so that either one of the two systems can be placed in the focal plane of the telescope for making a measurement. The third system is placed on the back of the photometer (photomultiplier in Fig. 1) and makes simultaneous measurements with one of the systems mounted on the photometer slide. The field of view of the various detector systems is determined by circular apertures placed in the focal plane of the telescope. Interference filters, which define various wavelength regions, are placed on the filter wheel in front of the detection systems.

Figure 1

The infrared photometer is shown schematically. Both the signal and reference beams are f/16; the displacement between the beams is 5 cm. The "flip-in" mirror may be inserted to view a black body reference instead of the sky.

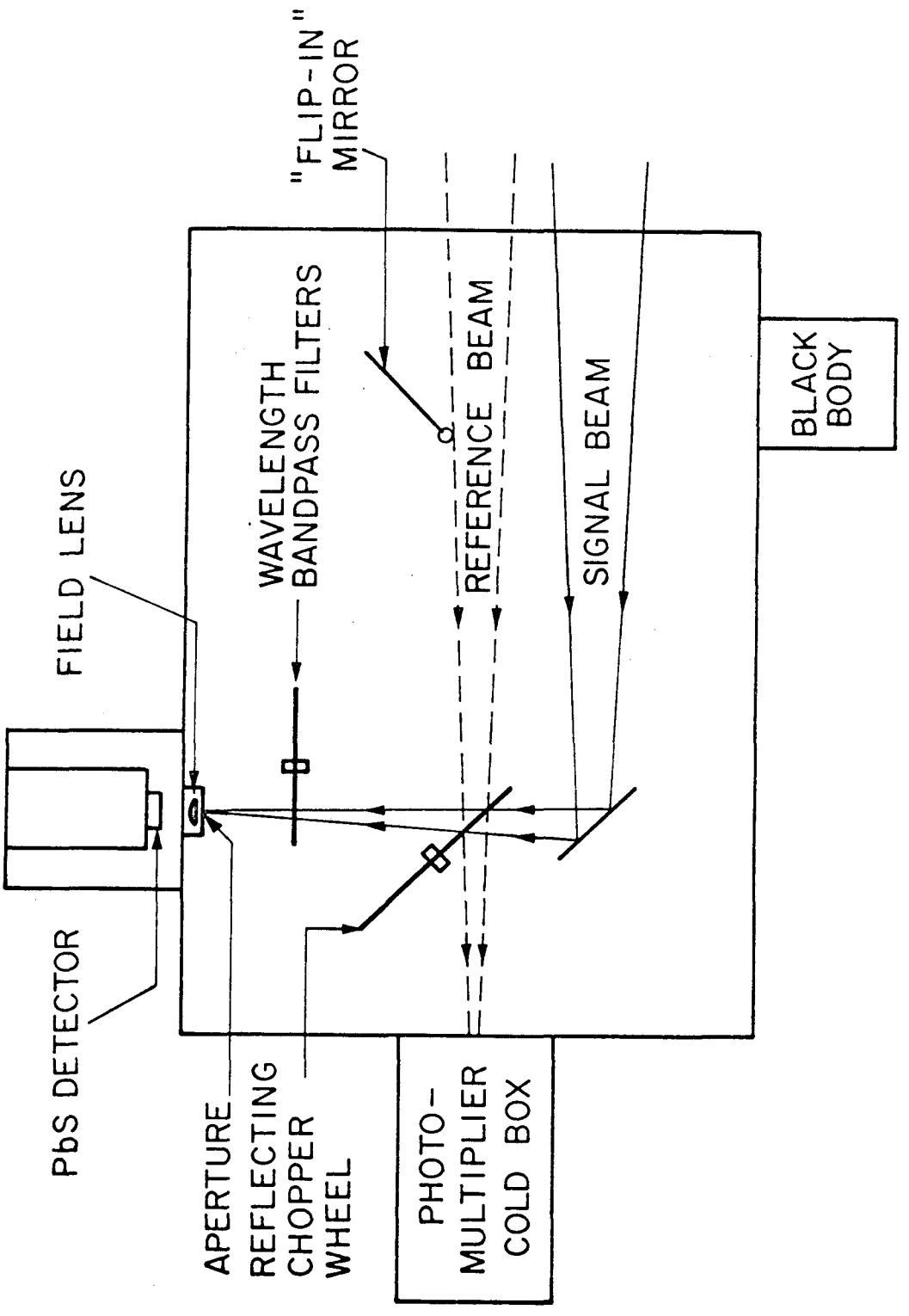
"FLIP-IN" MIRROR
WAVELENGTH BANDPASS FILTERS
REFERENCE BEAM
SIGNAL BEAM
BLACK BODY
FIELD LENS
PbS DETECTOR
APERTURE
REFLECTING CHOPPER WHEEL
PHOTO-MULTIPLIER COLD BOX

Figure 1

B. Detector Systems

Four infrared detection systems are used with the photometer; a summary of each is given in Table 1. The two PbS systems (1.4 - 2.6 μ, 3.1 - 3.8 μ) and the PbSe system (4.5 - 5.5 μ) are cooled to liquid nitrogen temperature, while the photomultiplier is cooled by dry ice. Since the noise of the PbS or PbSe system is proportional to the square root of the detector area, a very small detector (1/2 or 1/4 mm square) is used. To obtain a large flat field of view, the detector is placed behind an 8 or 4 mm field lens. Unwanted room temperature radiation, which lowers the sensitivity of the detector, is kept at a minimum by making the acceptance angle of the focused field lens the same as the f ratio of the telescopes (f/16) and by placing a cooled interference filter in front of the detector. Separate PbS systems are used at 2 and 3 μ because background radiation at wavelengths longer than 3 μ reduces the sensitivity of the 2 μ system by as much as a factor of 3.

The wavelength response of each system has been determined from the response curve of the detector supplied by the manufacturer and the transmission properties of the interference filter as measured on either a Cary 14 or a Beckman spectrophotometer. (Fig. 2 shows the transmission curve of the 2.0 to 2.4 μ filter.) According to data supplied by the filter manufacturers, the cooling of the interference filters causes a shift in the wavelength properties $\Delta\lambda/\lambda$ of less than 2%. The response characteristics of the five wavelength bands employed are shown in Table 2; the effects of atmospheric absorption normally expected while observing have been included, although the filters were

TABLE 1

INFRARED DETECTOR SYSTEMS

System	Detector	Cooling Temp. (°K)	Field Lens		Cooled Filter (μ)	System f Ratio
			Diam. (mm)	f Ratio		
1	1/2 x 1/2 mm PbS	77	8	1	1.4 - 2.6	16
2	1/4 x 1/4 mm PbS	77	4	1	3.1 - 3.8	16
3	1/2 x 1/2 mm PbSe	77	8	1	4.6 - 5.4	16
4	4 x 4 mm S-1 photomultiplier	194	10	4	None	10

Figure 2

The measured transmission properties of the 2.0 to 2.4 μ filter are shown. The vertical scale gives the fraction of the energy transmitted at each wavelength in arbitrary units. The horizontal scale is in microns. The curve was obtained on a Cary 14 spectrophotometer which has a resolution of 30 Å at 2.2 μ.

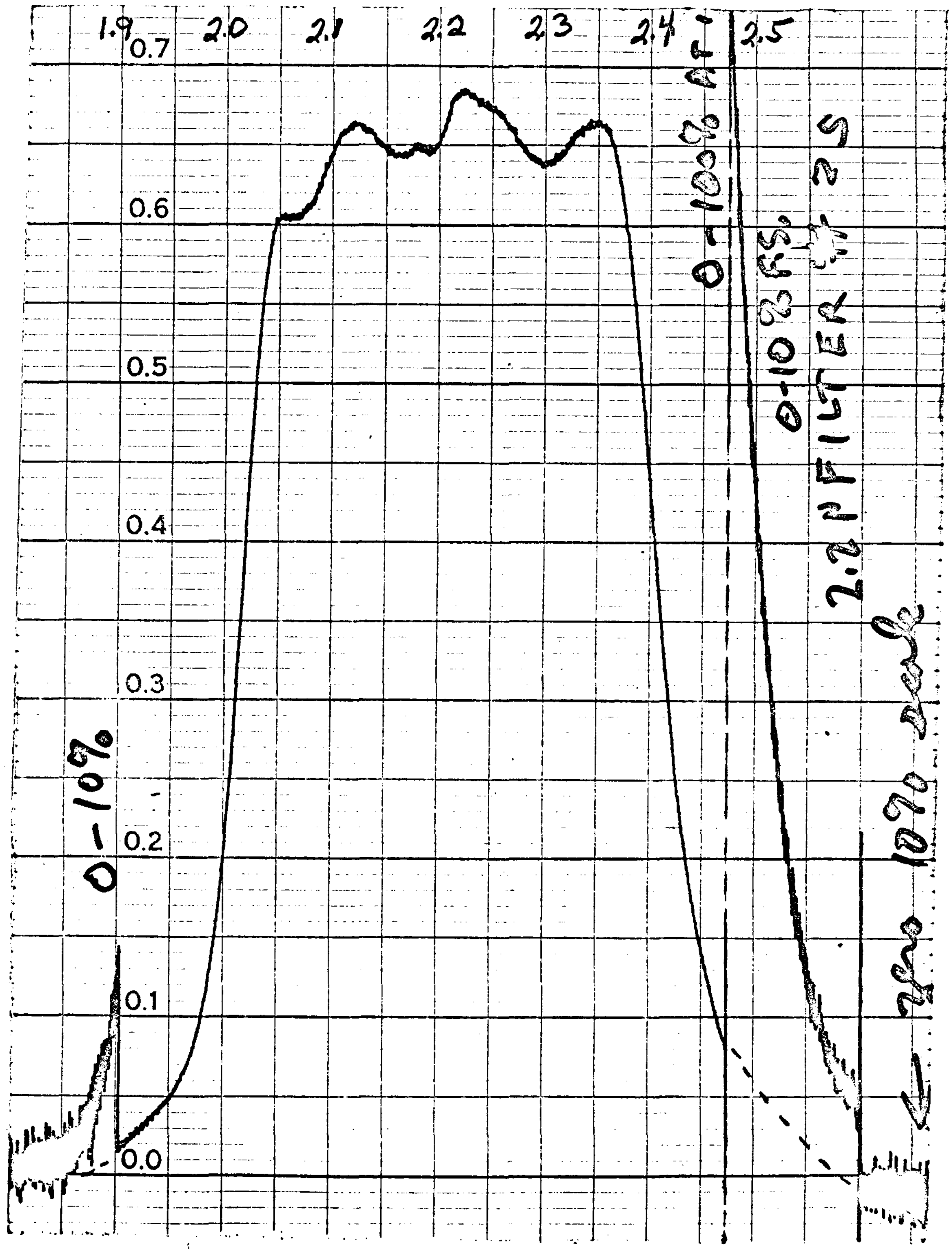
1.9
2.0
2.1
2.2
2.3
2.4
2.5
0.7
0.6
0.5
0.4
0.3
0.2
0.1
0.0
0-10%
0-100%
0-10% FS
2.2 μ FILTER
zero 10% scale

Figure 2

TABLE 2

PHOTOMETRIC RESPONSE CURVES

λ_e = 0.85 μ		λ_e = 1.65 μ		λ_e = 2.2 μ		λ_e = 3.4 μ		λ_e = 4.8 μ	
λ	R_λ	λ	R_λ	λ	R_λ	λ	R_λ	λ	R_λ
.70	.00	1.4	.00	1.90	.00	2.9	.00	4.5	.00
.75	.40	1.45	.11	1.95	.02	3.0	.05	4.6	.70
.80	1.00	1.50	.29	2.00	.17	3.1	.45	4.7	1.00
.85	.87	1.55	.53	2.05	.67	3.2	1.00	4.8	.90
.90	.60	1.60	.65	2.10	.89	3.3	.87	4.9	.65
.95	.40	1.65	.85	2.15	.91	3.4	.95	5.0	.60
1.00	.25	1.70	1.00	2.20	.91	3.5	1.00	5.1	.45
1.05	.15	1.75	1.00	2.25	1.00	3.6	.66	5.2	.25
1.10	.05	1.80	.06	2.30	.91	3.7	.66	5.3	.10
1.15	.00	1.85	.00	2.35	.78	3.8	.45	5.4	.02
				2.40	.33	3.9	.22	5.5	.00
				2.45	.09	4.0	.03		
				2.50	.00	4.1	.00		

chosen to minimize atmospheric attenuation (see Appendix A). All of the systems were checked on a Leiss Monochromator whose relative response and wavelength calibration were determined from an uncalibrated thermocouple and known atomic emission lines respectively. If the assumption is made that the energy response of the thermocouple is independent of wavelength, then the monochromator measurements agree with the data in Table 2 to within 20%. In addition, the monochromator measurements indicate that there is no significant energy response outside the wavelength regions of interest. For example, outside the wavelength band of each system the energy response, averaged over the resolution element of the monochromator ($\sim$ 0.1 μ), is always less than 0.1% of the energy response at the center of the bandpass.

The profile response of each system was checked on the telescope by scanning a star across the diameter of the lens; Fig. 3 shows a typical 2.2 μ scan across α Cyg taken on the 24-inch telescope. From the telescope scans it has been found that the profiles of all the systems are flat to within $\pm$5% rms. To further check the profile of the 1.4 - 2.6 μ system, the lens was completely mapped in the laboratory by using a point source of radiation focused on the lens. The results of this test showed that no position on the lens gave an output which varied from the average output by more than 10%.

The linearity of the detector response, as a function of radiant energy falling on the detector, has been checked both in the laboratory using a known temperature black body and on the telescope using Johnson and Morgan's (13) unreddened A0V stars. Table 3 shows,

Figure 3

A declination scan of α Cyg across the center of the 6 mm 2.2 μ entrance aperture is shown. The scan was made using the 24-inch telescope on 9 August 1966. The x scale is 0.42 arc min per division.

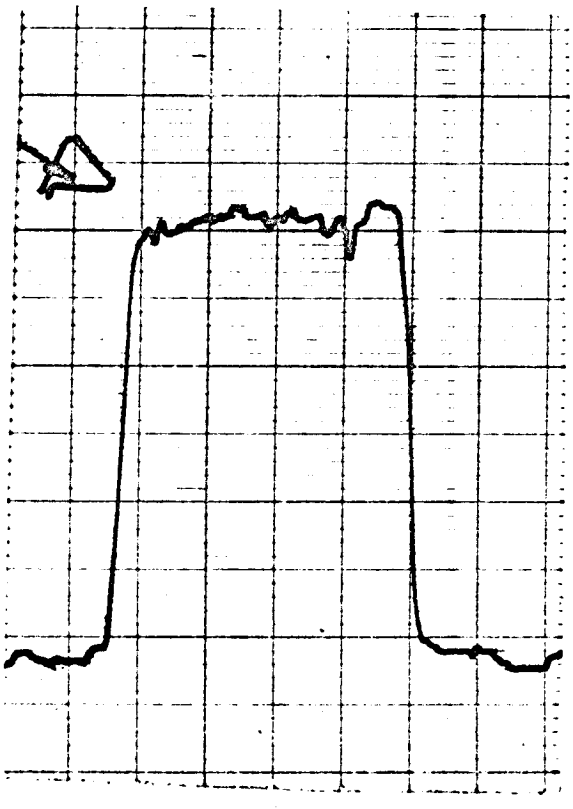

Figure 3

TABLE 3

2.2 μ PHOTOMETRY OF A0V STARS

Star	Normalized 2.2 μ Deflection*/0.54 μ Deflection (16)	Relative 2.2 μ Def.
α Lyr	1.00 ± .07	1000
α CrB	1.04 ± .07	140
γ Oph	1.04 ± .07	40
109 Vir	0.98 ± .07	33
BS 6070	0.99 ± .10	13
BS 5859	0.95 ± .12	5.4

*Data taken by Ted Hilgeman on the 24-inch telescope 13 July 1966.

for several A0V stars, the normalized ratio of the 2.2 μ deflection as measured with a PbS detector to the 0.54 μ deflection as measured with a 1P21 photomultiplier by Johnson (16). The fact that all stars show the same ratio indicates the PbS detector is as linear as a 1P21 photomultiplier over a dynamic range of 200. Furthermore, a comparison of measurements made on the 24- and 200-inch telescopes showed that the PbS detectors are linear to within 5% over the complete 10^5 dynamic range used.

C. Electronics

The principle features of the electronic system are briefly outlined below. The PbS and PbSe detectors are biased with 50 volts d.c. When modulated radiation (produced by the chopping procedure outlined above) falls on the detector an a.c. voltage is produced which is normally between 10 and 10^6 microvolts. This a.c. voltage is first amplified and then multiplied by an in-phase synchronous square wave obtained photoelectrically from the modulating chopper blade. The resultant d.c. voltage, which is directly proportional to the radiant energy, independent of system noise, is then displayed in analog form on a strip chart recorder. Further details of the electronic system are given by Westphal, Murray and Martz (14).

It should be noted that radiation present in the reference beam will produce an a.c. voltage 180 degrees out of phase with respect to the voltage produced by radiation in the signal beam; therefore with this electronic system, radiation in the reference beam produces a negative deflection on the recorder.

III. OBSERVATIONS

Observations of the galactic center region were made in the wavelength bands 0.75 - 1.1 μ (λ effective = 0.85 μ), 1.5 - 1.8 μ (λ effective = 1.65 μ), 2.0 - 2.4 μ (λ effective = 2.2 μ), 3.1 - 3.8 μ (λ effective = 3.4 μ), and 4.6 - 5.4 μ (λ effective = 4.8 μ); the most extensive and highest quality data are those made in the 2.0 - 2.4 μ band.

The data were obtained with the photometer mounted at the f/16 Cassegrain focus of the 24-, 60-, or 200-inch reflecting telescopes of the Mount Wilson and Palomar Observatories. This range of telescope apertures, when used with either a 6, 4, 2, or 1 mm focal plane diaphragm, resulted in resolutions ranging from 1.8 to 0.04 arc min.

Table 4 lists the observations made during 1966 and 1967, with the exception of the data discussed in Appendix B.

Most of the 2.2 and 1.65 μ data were obtained from right ascension and declination scans. For this type of observation the telescope was scanned across the sky at a known rate; the relative position of the telescope in the sky was recorded simultaneously with the infrared signal. The scanning rate that was used varied depending upon the observation; usually a scan took 3 to 5 minutes of time to complete. To maximize the signal to noise ratio the response time of the electronic system was usually about 1/5 the time required for a star to pass across the diameter of the aperture. Figures 4 and 5 show strip recordings of typical 2.2 μ scans of the galactic center region with

TABLE 4

RECORD OF OBSERVATIONS

Wavelength Region (μ)	Angular Resolution (arc min)	Telescope (inches)	Area Mapped (sq. arc min)	Number of Scans	Offset of Reference Field (arc min)	Dates
0.8 - 1.1	1.2	24	+	5	15 W	18, 20 Aug. '66
0.8 - 1.1	0.17	200	+	5	2 S	6 Sept. '66
1.5 - 1.8	1.8	24	+	6	15 W	9, 17, 20, 21 Aug. '66
1.5 - 1.8	0.8	60	+	2	7 N	25 Aug. '66
1.5 - 1.8	0.6	24	+	*	15 W	21 Aug. '66
1.5 - 1.8	0.25	200	+	3	2 S	7 Sept. '66
1.5 - 1.8	0.08	200	+	1	2 S	6 Sept. '66
2.0 - 2.4	1.8	24	1000	60	15 W	9, 10, 17, 18, 19, 20 Aug. '66
2.0 - 2.4	1.8	24	500	20	Constant Temp.	21 Aug. '66
2.0 - 2.4	0.8	60	100	29	7 N	23, 24, 25, Aug. '66 and 29 May '67
2.0 - 2.4	0.6	24	+	*	15 W	21 Aug. '66
2.0 - 2.4	0.26	60	+	1	7 N	25 Aug. '66
2.0 - 2.4	0.25	200	30	18	2 S	5, 6, 7 Sept. '66
2.0 - 2.4	0.08	200	+	10	2 S	6, 7 Sept. '66 and 26 Aug. '67
2.0 - 2.4	0.04	200	+	1	.5 N	29 June '67

TABLE 4--Continued

Wavelength Region (μ)	Angular Resolution (arc min)	Telescope (inches)	Area Mapped (sq. arc min)	Number of Scans	Offset of Reference Field (arc min)	Dates
3.1 - 3.8	0.8	60	+	*	7 N	29 May '67
3.1 - 3.8	0.26	60	+	*	7 N	25 Aug. '66
3.1 - 3.8	0.25	200	+	*	.5 N	26 Aug. '67
3.1 - 3.8	0.08	200	+	*	.5 N	26 Aug. '67
4.6 - 5.4	0.08	200	+	*	.5 N	13, 14, 25 Sept. '67

+Indicates that systematic mapping was not attempted.

*Indicates that data were not taken in the form of scans.

Figure 4

A strip chart recording of a right ascension scan of the galactic center region at 2.2 μ obtained with the 24-inch telescope on 18 August 1966 using an aperture of 1.8 arc min is shown. In this trace at Dec. = -28° 59.5', there is an out of focus reference beam 15 arc min to the west in the sky. 1 cm in the figure is equivalent to $3.0 \pm 0.3 \times 10^{-19}$ W m^{-2} Hz^{-1} $ster^{-1}$. West is to the left. The tracing of γ Sagittarii was obtained with the same scanning rate and time constant, but with the amplifier gain reduced by a factor of 6.3.

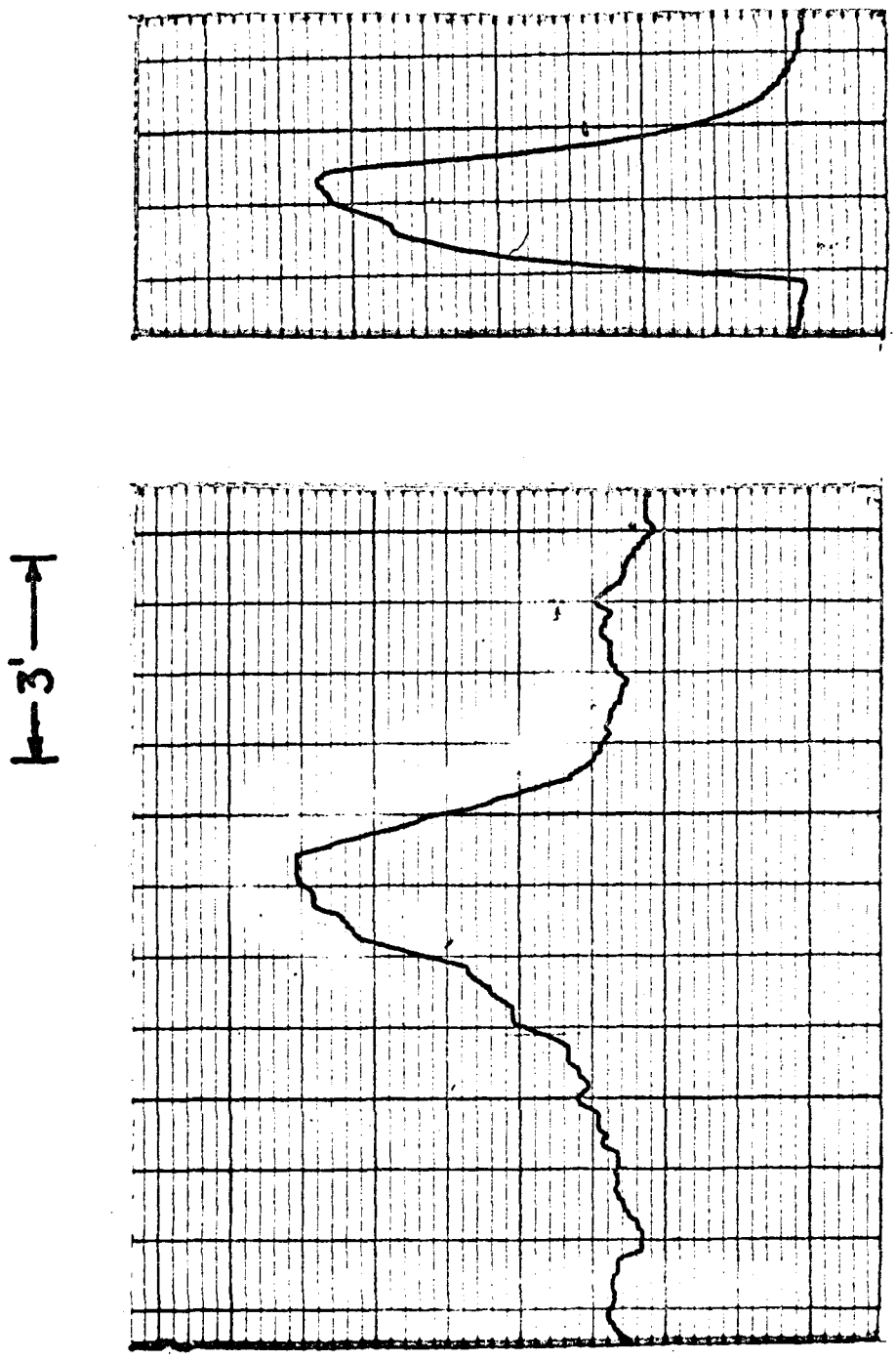

Figure 4

Figure 5

Strip chart recordings of right ascension and declination scans of the galactic center region and of γ Sagitarii at 2.2 μ obtained with the 200-inch telescope using an aperture of 0.08 arc min are shown. The right ascension and declination scan rates in the sky are the same. The right ascension scans were made at the declinations labeled A and B. The amplifier gain was the same for all scans of the galactic center region and was reduced by a factor of 320 for γ Sagitarii. 1 cm in the figure is equivalent to $6.0 \pm 0.5 \times 10^{-18}$ W m^{-2} Hz^{-1} $ster^{-1}$. For the declination scan north is to the left, and for the right ascension scans west is to the left.

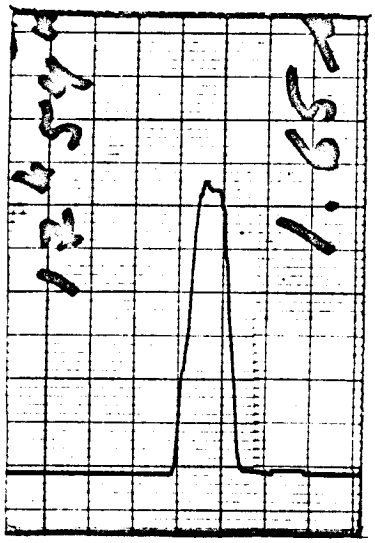

R.A. SCAN γ SGR.

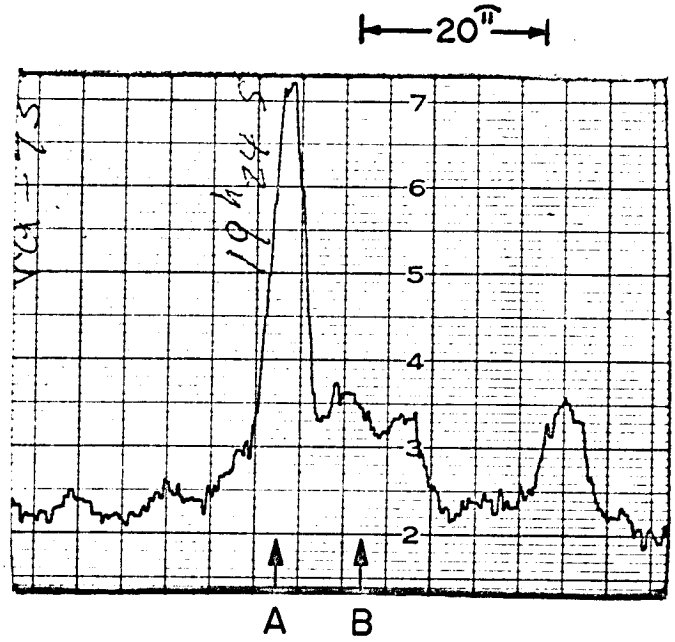

DEC. SCAN

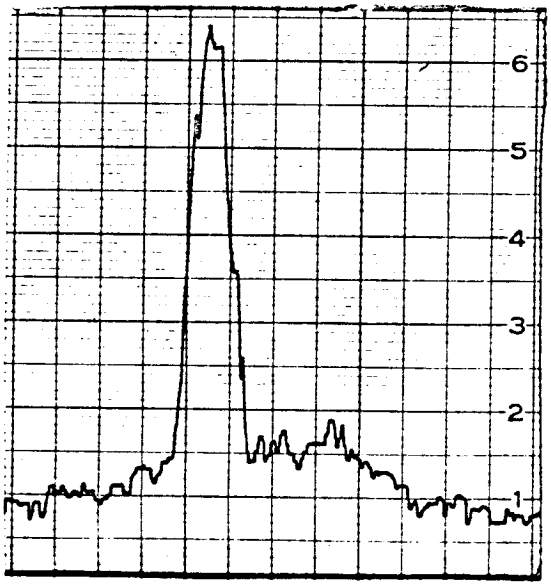

R.A. SCAN (A)

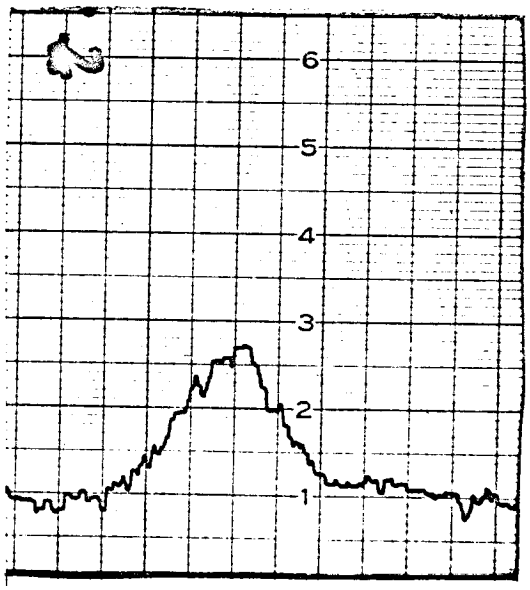

R.A. SCAN (B)

Figure 5

1. 8 and 0. 08 arc min resolution. It should be noted that the reference beam for all scans, except those taken on 21 August 1966, was a near-by area of the sky, while on 21 August 1966 the scans had a constant temperature black body reference. At 2. 2 μ more than 1000 square arc min of the galactic center region were covered by telescope scans with a resolution of 1. 8 arc min. The 2. 2 μ coverage at other resolutions and the 1. 65 μ coverage are shown in Table 4.

The true position of the telescope in the sky, as well as the response characteristics of the detection systems were determined by scanning across a standard star (15, 16) approximately every half hour. It almost all cases γ Sagittarii was used as the standard star, however, 1 to 5 secondary standards were also observed each night.

Telescope scans were not attempted at 3. 4 and 4. 8 μ because of the low signal to noise ratios. For measurements made at these wavelengths, as well as for some made at 2. 2 and 1. 65 μ, the radiation within a fixed region was measured. This type of observation was possible because, regardless of the angular resolution, there was always a position in the sky which had a well defined maximum signal output. At 2. 2 μ the position in the sky which gave the maximum signal was easy to determine, and a measurement of the radiation present was made by comparing the deflection at this position to the deflection from a portion of the sky where the radiation was taken to be zero. At 3. 4 and 4. 8 μ the signal to noise ratios were not always large enough to position the telescope correctly, so it was necessary to position the telescope with the 2. 2 μ system. Then, by means of the photometer slide discussed in section II, the 2. 2 μ system was quickly replaced

by either the 3.4 or 4.8 μ system (see Fig. 6 for a sample of a 3.4 μ measurement). The 2.2 μ system used for positioning the telescope always had a focal plane entrance aperture equal to, or smaller than, the long wavelength aperture; therefore correct positioning of the telescope was assured. This procedure of positioning the telescope with the 2.2 μ system was repeated 25 times at 4.8 μ before a signal three times larger than the noise was obtained; calibration checks were made to show that no spurious signals were produced by long period drifts or by movements of the telescope. Table 6 (page 46) shows the apertures and wavelengths for which observations of this type were made.

Although radiation was not detected at 0.85 μ, upper limits on the radiation present were obtained from 0.85 μ scans taken simultaneously with 2.2 μ scans.

Figure 6

A sample of a 3.4 μ measurement taken with the 200-inch telescope on 26 August 1967 using 0.25 arc min resolution is shown. The telescope was positioned in the sky with the help of the 2.2 μ system (see text for an explanation).

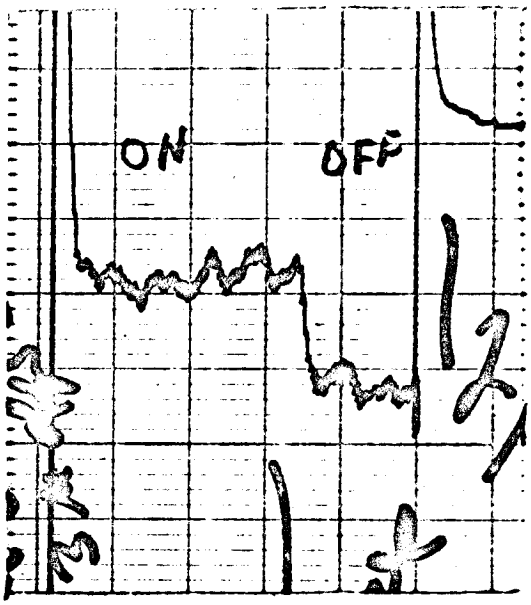

Figure 6

IV. REDUCTION OF DATA

All the observed deflections measured in the galactic center region have been reduced to flux densities (W m^{-2} Hz^{-1}) by means of the observed standard stars and the absolute calibration discussed in Appendix A. By using the measured area of the focal plane apertures shown in Table 4, the flux densities were converted into surface brightnesses (W m^{-2} Hz^{-1} $ster^{-1}$) as a function of position in the sky.

In this paper the flux densities and surface brightness distributions at various wavelengths are presented in three different ways: a) as right ascension and declination profiles, b) as brightness distribution contour maps, and c) in tabular form.

Typical scan profiles at 2.2 μ are shown in Figs. 4, 5, 7a, and 7b. Figures 4 and 7a are actual right ascension scans made on the 24-inch telescope with 1.8 arc min resolution; Fig. 7a was obtained with a constant temperature black body reference while Fig. 4 had the reference beam 15 arc min west of the signal beam in the sky. Figure 4 is a scan directly across the maximum of the source, while Fig. 7a shows the profile 2 arc min south of the maximum. (Note the difference in both the x and y scale of the two figures.) Figure 7b shows two right ascension scans taken at the 60-inch telescope using a 0.8 arc min aperture. In the figure the profiles have their reference beam 7 arc min north of the signal beam in the sky. Scans taken with the 200-inch telescope with 0.08 arc min resolution are given in Fig. 5. The profiles were taken in the vicinity of the maximum signal from the source; the reference beam was 2 arc min south of the signal beam.

Figure 7a

A strip chart recording is shown of a right ascension scan of the galactic center region at 2.2 μ obtained with the 24-inch telescope on 21 August 1966 using an aperture of 1.8 arc min. In this trace, which was made at the delination - 29°01.5', a constant temperature black body reference beam was used. 1 cm deflection in the figure is equivalent to $1.6 \pm 0.2 \times 10^{-19}$ W m^{-2} Hz^{-1} $ster^{-1}$. The right ascension scale shown is in minutes of time (1 min of time = 13 arc min) with west to the left. The right ascension coordinate is for 1966; a 1950 coordinate is obtained by subtracting 1.05 minutes of time.

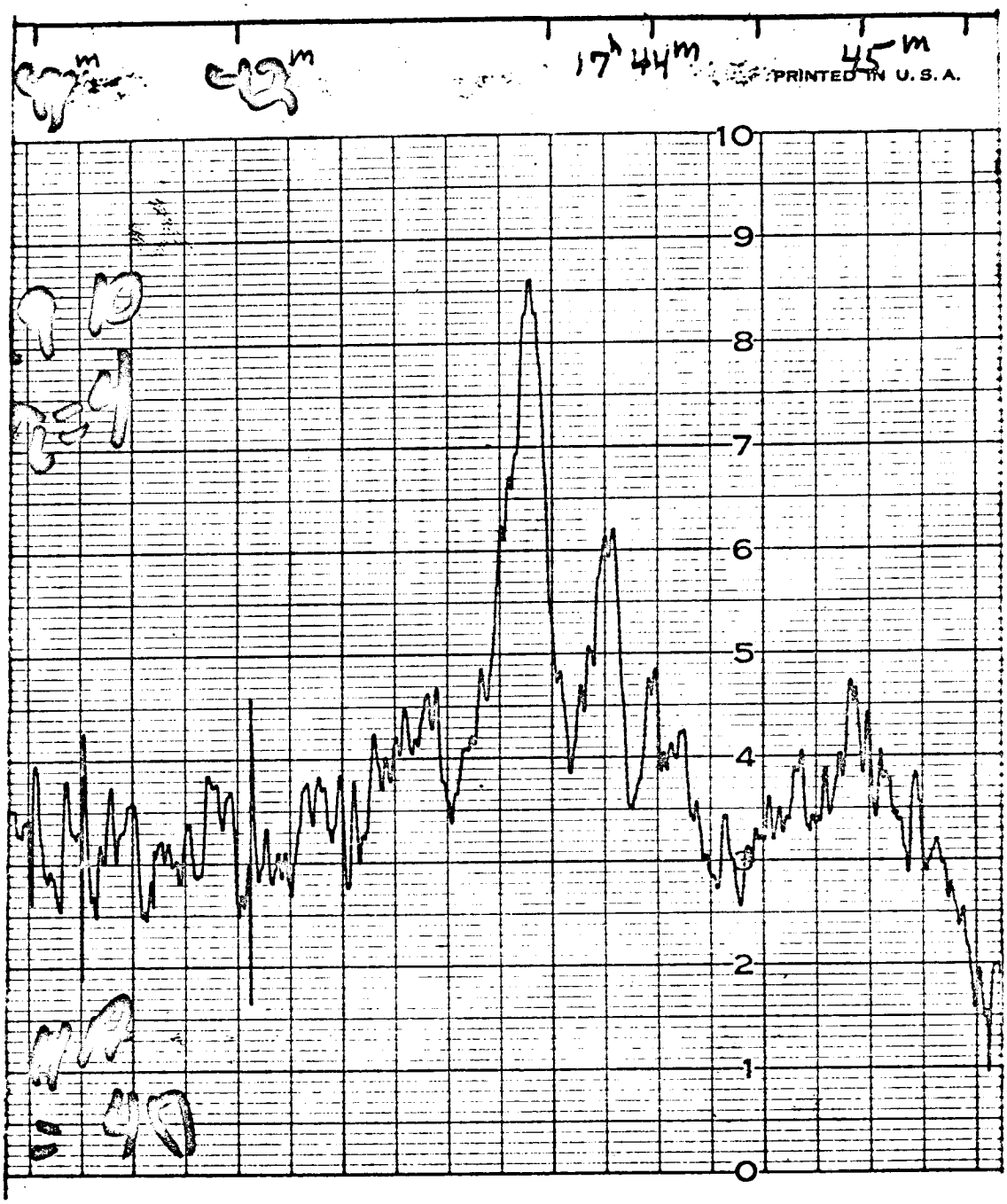

Figure 7a

Figure 7b

Two strip chart recordings of right ascension scans of the galactic center region at 2.2 μ obtained with the 60-inch telescope on 24 August 1966 using an aperture of 0.8 arc min are shown. For these scans there is an out of focus reference beam 7 arc min north in the sky. 1 cm deflection in the figure is equivalent to $6.0 \pm 0.6 \times 10^{-19}$ W m^{-2} Hz^{-1} $ster^{-1}$. West is to the left. The tracing of τ Sagittarii was obtained with the same scanning rate and time constant, but with the amplifier gain reduced a factor of 16.

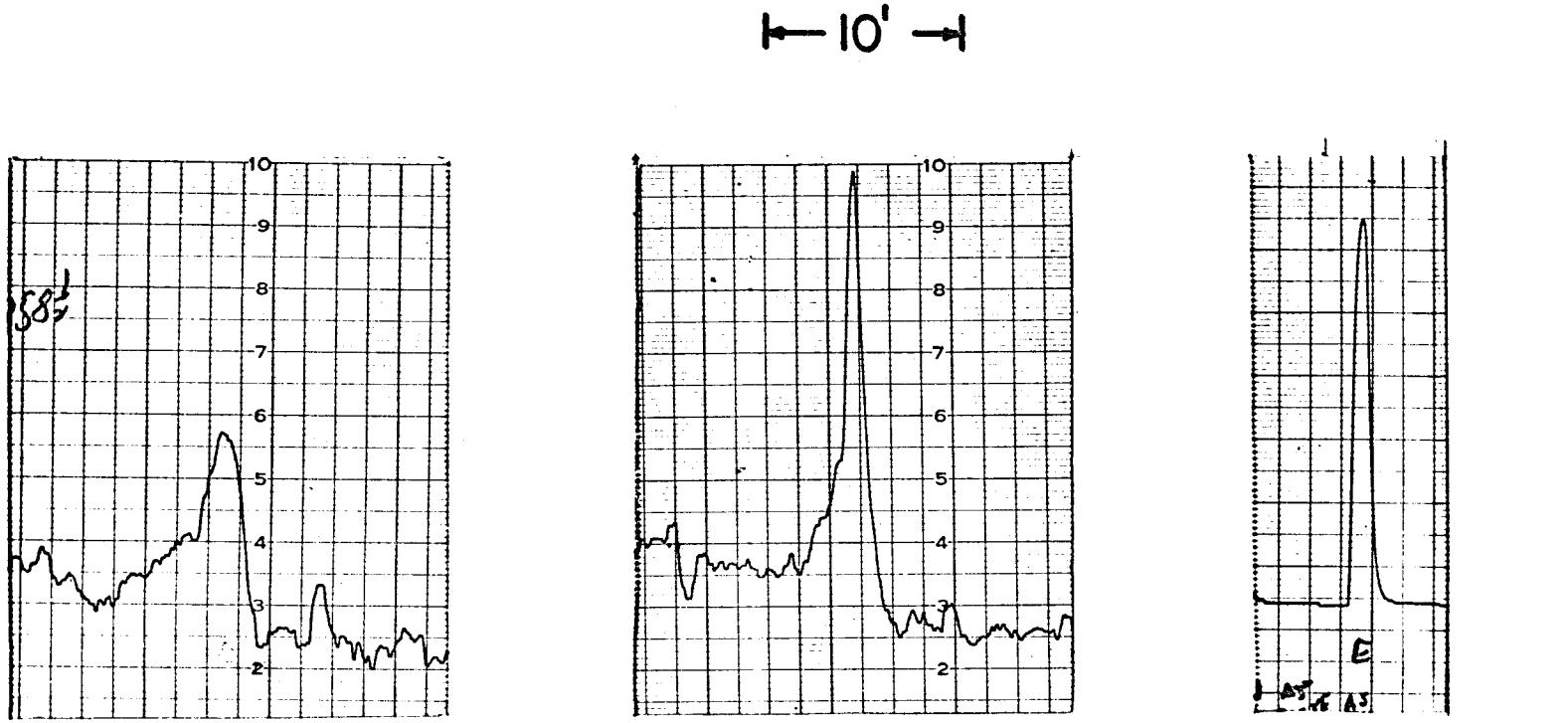
10'
10
9
8
7
6
5
4
3
2
R. A. Scan, dec. = −28°59.0'
R. A. Scan, dec. = −28°59.5'
R. A. Scan, τ Sgr.

Figure 7b

A sufficient number of right ascension and declination scans were made at 2.2 μ to permit construction of the brightness distribution contour maps shown in Figs. 8, 9 and 10 with resolutions of 1.8, 0.8 and 0.25 arc min, respectively.

Figure 8 is a contour map of the galactic center region constructed from the data obtained on the 24-inch telescope with 1.8 arc min resolution. The basic structure presented in the map was determined from the observations of 21 August 1966 when a constant temperature black body was used in the reference beam; therefore, the output deflection was a direct measure of the radiation in the signal beam (the trace in Fig. 7a is characteristic of the scans taken on 21 August 1966). On 21 August 1966, ten different right ascension profiles, separated by 2 arc min in declination, were observed; each profile consisted of two independent telescope scans. The profiles were put into digital form in terms of deflection versus declination and right ascension. The digitizing was done in units of approximately 1/20th the maximum deflection, which was also the approximate size of the uncertainty in the profiles. The digitized profiles were then placed on a right ascension-declination grid by means of numerical symbols.

In addition to the ten profiles taken on 21 August 1966, other 24-inch scans were also added to the grid. All of these additional profiles had a reference beam 15 arc min west of the signal beam in the sky. When all available data were placed on the grid, it was found that over 90% of the area was covered once or more, and over 50% of the area was covered twice or more.

Figure 8

A contour map of the galactic center region at 2.2 μ taken with an aperture of 1.8 arc min diameter is presented. Contour lines are separated by 8.5×10^{-20} W m^{-2} Hz^{-1} $ster^{-1}$ (5.2×10^{-10} W cm^{-2} μ^{-1} $ster^{-1}$) and are uncertain by about the same amount. An "X" represents a point-like source.

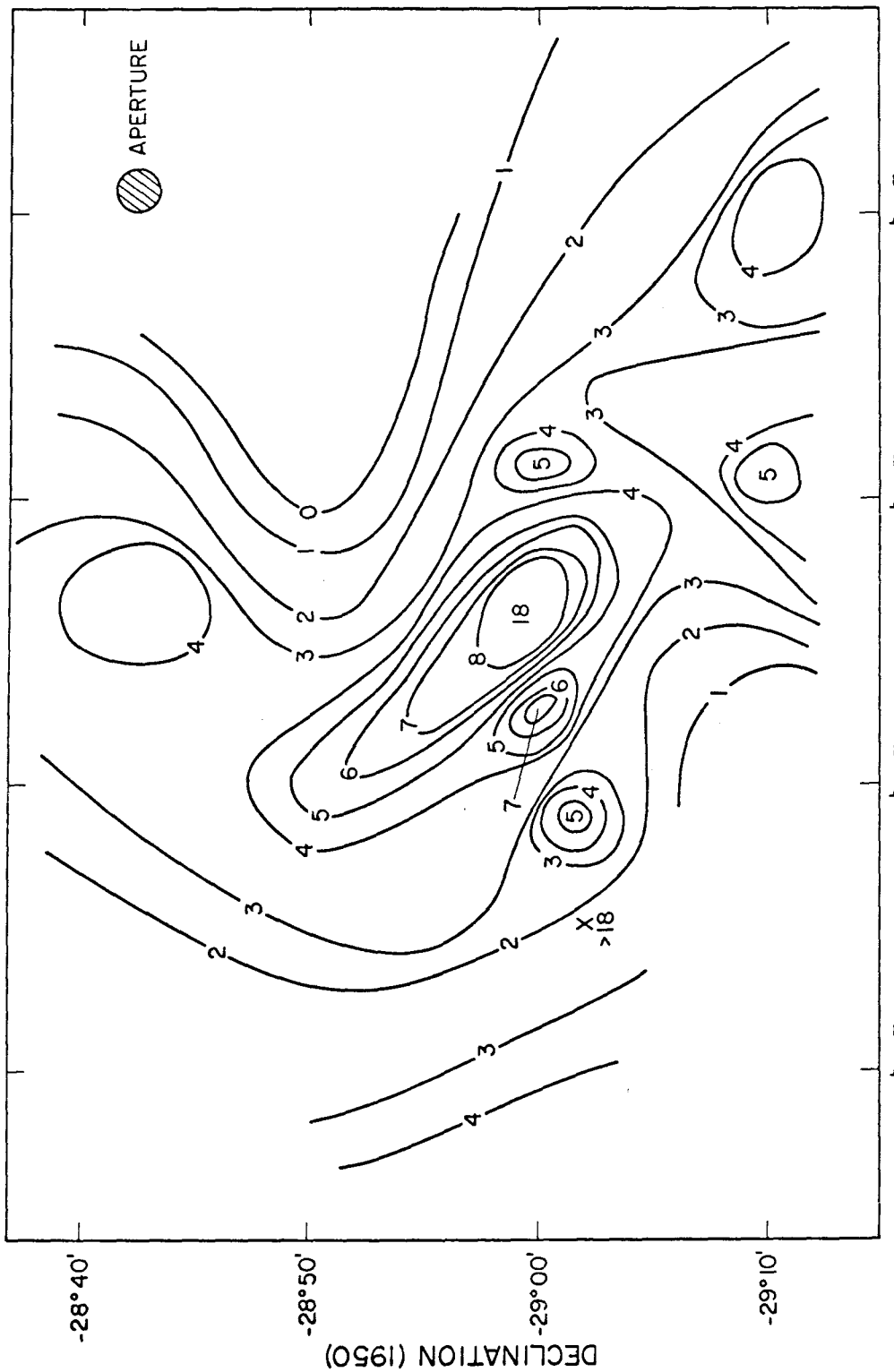
APERTURE
DECLINATION (1950)
-28°40'
-28°50'
-29°00'
-29°10'
RIGHT ASCENSION (1950)
17h44m
17h43m
17h42m
17h41m
X
>18

Figure 8

Figure 9

A contour map of the galactic center region at 2.2 μ taken with an aperture of 0.8 arc min diameter is given. Contour lines are separated by 1.7×10^{-19} W m^{-2} Hz^{-1} $ster^{-1}$ and are uncertain by about the same amount. The position of each scan is shown by a dashed line. An "X" represents a point-like source.

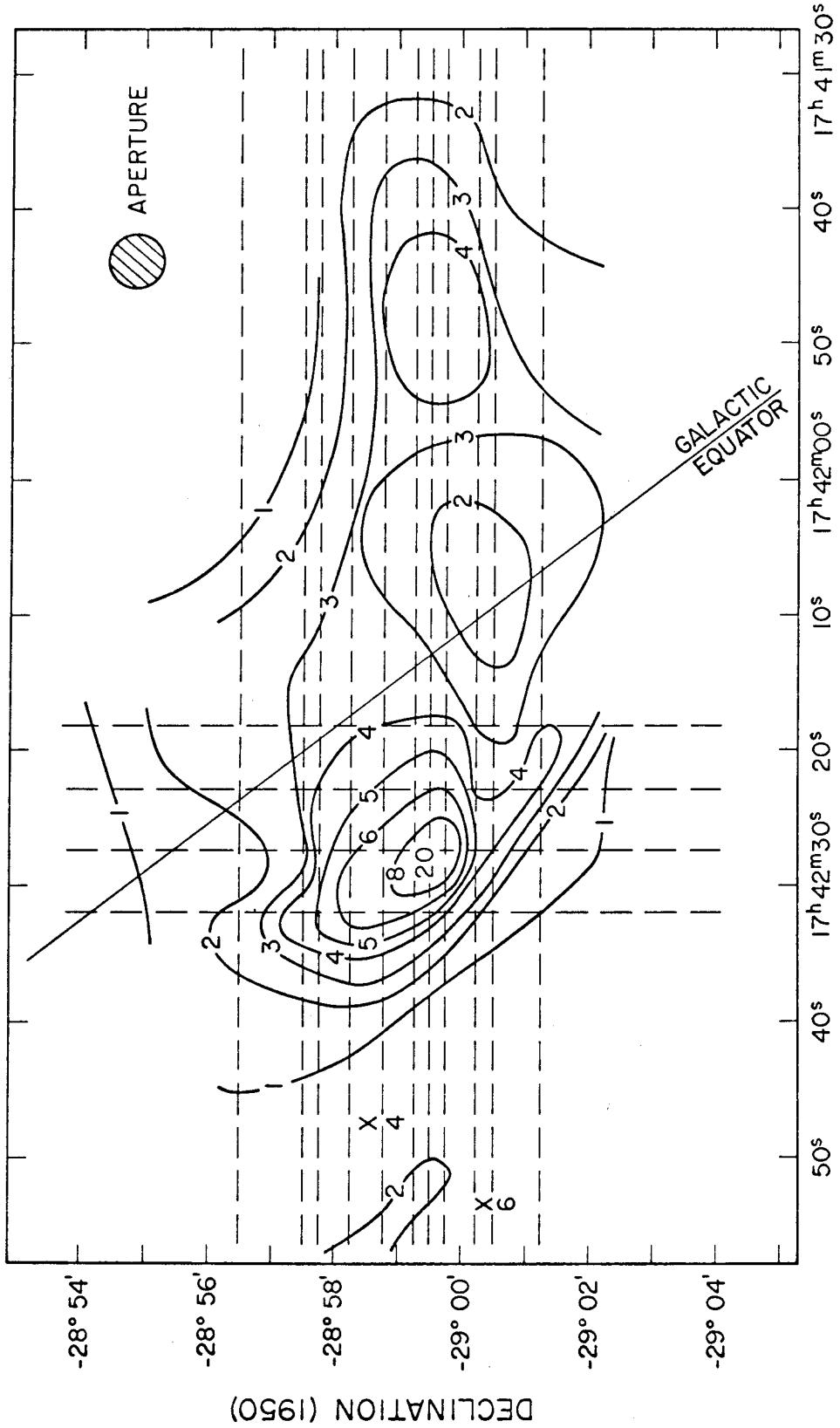
APERTURE
GALACTIC EQUATOR
RIGHT ASCENSION (1950)
DECLINATION (1950)
17h41m30s
40s
50s
17h42m00s
10s
20s
17h42m30s
40s
50s
-28° 54'
-28° 56'
-28° 58'
-29° 00'
-29° 02'
-29° 04'

Figure 9

Figure 10

A contour map of the galactic center region at 2.2 μ taken with an aperture of 0.25 arc min diameter is given. Contour lines are labeled in units of 1.6 x 10^{-19} W m^{-2} Hz^{-1} $ster^{-1}$ and are uncertain by about the same amount. The unlabeled contours in the center have values 10, 12, 14, and 16 respectively. The position of each scan is shown by a dashed line.

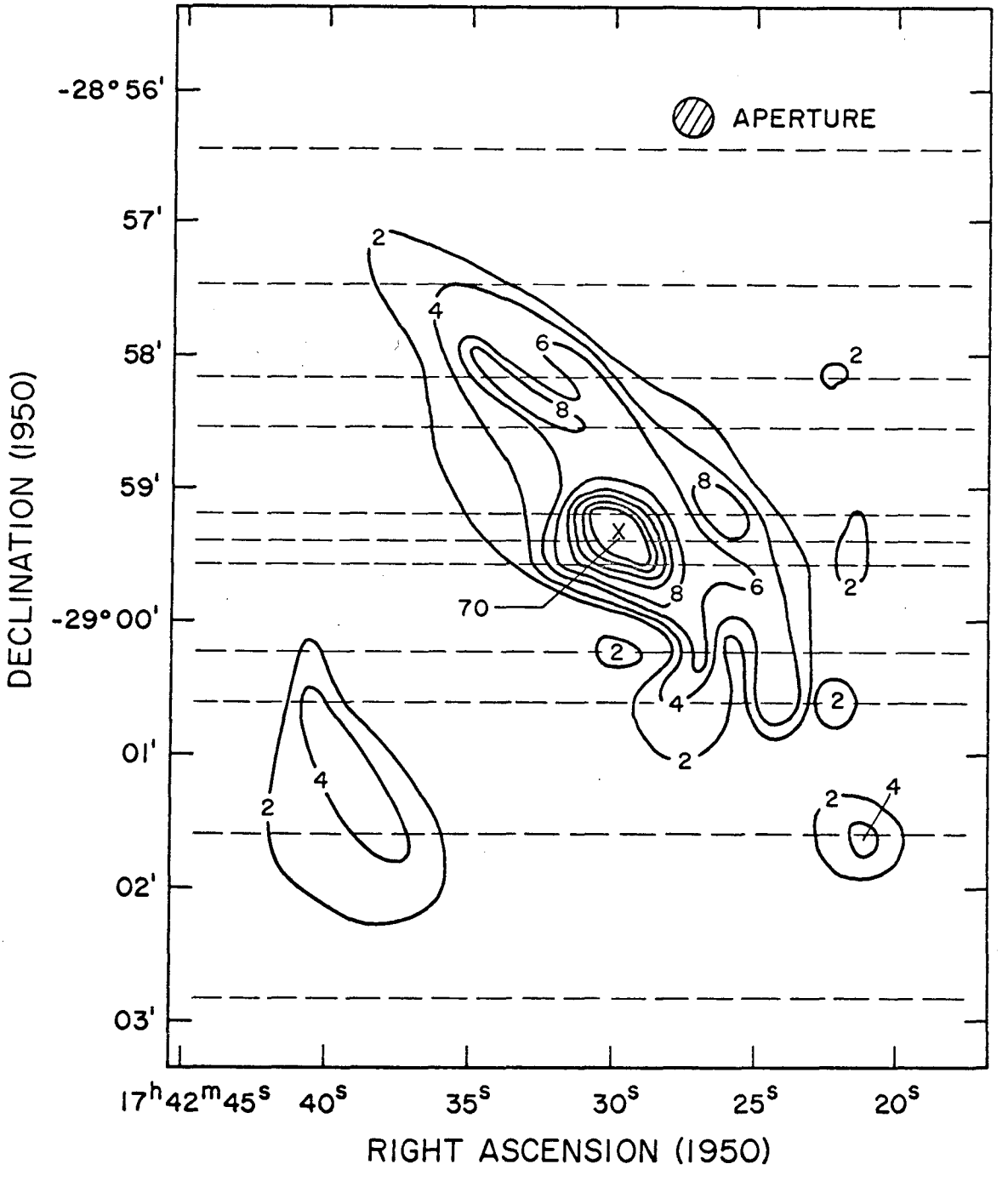
APERTURE
-28° 56'
57'
58'
59'
-29° 00'
01'
02'
03'
DECLINATION (1950)
17h 42m 45s
40s
35s
30s
25s
20s
RIGHT ASCENSION (1950)
2
4
6
8
70

Figure 10

Smooth contour lines were drawn on the grid which passed through positions of equal deflection. When there was a region in which several different deflections were available, an average of the deflections was taken, with the highest weight given to the data from the 21 August 1966. The final contours agreed with the digitized deflections to within an rms deviation of less than the separation of the contours; for example, the traces in Figs. 4 and 7a are right ascension profiles at Dec = - 28° 59.5' and Dec = - 29° 01.5' in Fig. 8.

Figure 9 is the contour map drawn from the data obtained on the 60-inch telescope with 0.8 arc min resolution. The map was constructed from 29 profiles similar to those shown in Fig. 7b. The procedure used was the same as described for Fig. 8. The uncertainty in each of the profiles used was less than 5% of the maximum signal; however, the uncertainty in the adopted contours is about ± 10% (compare the data in Fig. 7b with data in Fig. 9). The reference beam for the data in this map was always 7 arc min north of the signal beam. In constructing the map, possible radiation in the reference beam was neglected. How much radiation was actually in the reference beam can be estimated from a scan taken 7 arc min north of the maximum signal. The largest deflection on this scan was 2 contour divisions.

Figure 10 is a contour map of the galactic center made up from the data taken on the 200-inch telescope with 0.25 arc min resolution. The map was constructed by G. Neugebauer in basically the same way as the previously described maps. The uncertainty in the map is about ± 5% of the maximum signal shown. The reference beam was 2.2 arc min south of the signal beam. Several scans were taken

at the position which the reference beam had when the signal beam was on the source. From these scans a slight correction was made for radiation in the reference beam; the error caused by the presence of the reference beam has been estimated to be less than 5% of the maximum signal shown.

Because the emission from the telescope and sky varies with the position of the telescope, the true zero of energy of each map can be determined only if it is possible to observe a region in the sky which is close to the source and which is known to have no emission. The extended nature of the center of the Galaxy precluded such a measurement; therefore, for each map a local zero of energy was chosen near the edge of that map.

For these maps no attempt was made to compensate for the effects of the finite resolutions. Therefore the maps represent the actual brightness distribution in the sky convolved with a flat circular beam with square edges (see Fig. 3). (The system response time also causes a distortion of the maps along the scanning direction; however from two scans made with two different response times this distortion was found to be negligible compared to the features shown on the maps.)

Although many scans were made in the region of the galactic center at 1.65 μ, the signal to noise ratio of these scans was not large enough to permit construction of reliable contour maps. For this reason the 1.65 μ data are given in Table 5 as the average ratio of 1.65 μ to 2.2 μ surface brightness [$B_\nu(1.65)/B_\nu(2.2)$]. The table is divided into sections according to the approximate position of each datum point. The ratios have been obtained by numerically integrating the total

TABLE 5

OBSERVED COLOR RATIOS

Coordinates of Observation		Resolution (arc min)	$B_\nu(1.65)/B_\nu(2.2)$
Right Ascension (1950)	Declination (1950)		
$17^h\ 42^m\ 18^s$ to $17^h\ 42^m\ 42^s$	$-28^\circ\ 59.3'$	1.8	$0.18 \pm .05$
$17^h\ 42^m\ 15^s$ to $17^h\ 42^m\ 45^s$	$-28^\circ\ 58.3'$	0.8	$0.24 \pm .03$
$17^h\ 42^m\ 30^s$	$-29^\circ\ 01'$ to $-28^\circ\ 57'$	0.8	$0.18 \pm .02$
$17^h\ 42^m\ 21^s$ to $17^h\ 42^m\ 39^s$	$-28^\circ\ 59.3'$	0.25	$0.25 \pm .02$
$17^h\ 42^m\ 25^s$ to $17^h\ 42^m\ 35^s$	$-28^\circ\ 59.0'$	0.25	$0.20 \pm .02$
$17^h\ 42^m\ 25^s$ to $17^h\ 42^m\ 35^s$	$-28^\circ\ 59.6'$	0.25	$0.15 \pm .02$
$17^h\ 42^m\ 27^s$ to $17^h\ 43^m\ 03^s$	$-28^\circ\ 57.3'$	1.8	$0.29 \pm .06$
$17^h\ 42^m\ 42^s$	$-28^\circ\ 58'$ to $-28^\circ\ 54'$	1.8	$0.33 \pm .05$
$17^h\ 41^m\ 53^s$	$-29^\circ\ 00'$	1.8	$0.55 \pm .15$
$17^h\ 41^m\ 40^s$ to $17^h\ 42^m\ 10^s$	$-29^\circ\ 00'$	0.8	$0.50 \pm .15$
$17^h\ 42^m\ 44^s$	$-29^\circ\ 00'$	1.8	$0.55 \pm .15$
$17^h\ 44^m\ 00^s$	$-28^\circ\ 57'$	1.8	$0.45 \pm .08$
			$B_\nu(0.9)/B_\nu(2.2)$
$17^h\ 42^m\ 28^s$ to $17^h\ 42^m\ 32^s$	$-28^\circ\ 59.3'$	0.17	< 0.001
$17^h\ 42^m\ 20^s$ to $17^h\ 42^m\ 40^s$	$-28^\circ\ 59'$	1.2	< 0.01

deflection of two coincident 1.65 and 2.2 μ scans over the region shown in columns 1 and 2 of Table 5. The zero of the two deflections was always taken at the edge of the scans, and should correspond roughly to the same zero as shown in the maps. If the 1.65 μ surface brightness in a given region is required, it is necessary to determine the 2.2 μ surface brightness from Figs. 8, 9, or 10 and then to multiply this surface brightness by the appropriate ratio given in Table 5. Also shown in Table 5 are the limits on the ratio $B_\nu(0.9)/B_\nu(2.2)$ which have been obtained in the same way as the 1.65 μ ratios.

Table 6 is a summary of the mean flux densities measured with different apertures centered on the position of maximum brightness, R.A. = $17^h\ 43.5^m$, Decl. = $-28^\circ\ 59.4'$; the energy at R.A. = $17^h\ 40^m$, Decl. = $-29^\circ\ 00'$ was arbitrarily taken to be zero.

For measurements made with apertures smaller than 0.8 arc min the zero position stated above was not included in the observations. To make the quoted flux densities have the proper zero, a small correction was applied. An additional correction for possible radiation in the reference field was also made. Both the correction to the proper zero and the correction for reference field were made with the help of Fig. 8 and were always less than 10% of the total value. The errors quoted in the table include cell and sky noise, uncertainty in the sensitivity, and an estimate of the error in the correction factors.

The final presentation of the data is shown in Fig. 11, where the flux density within an area of 3.5 arc min diameter centered on the position of maximum brightness is plotted as a function of frequency. The 2.2 μ point was obtained by integrating the data in Figs. 4 and 8,

TABLE 6

OBSERVED FLUX DENSITIES

Aperture Diameter (arc min)	Flux Density (10^{-26} W m^{-2} Hz^{-1})			
	1.65 μ	2.2 μ	3.4 μ	4.8 μ
0.04		1.5 ± 0.2[1]		
0.08	0.23 ± 0.05	1.7 ± 0.1[2]	5.3 ± 1.0[1]	4.0 ± 2.0[1]
0.25	0.79 ± 0.1	4.6 ± 0.2	14.0 ± 3.0[1]	
0.26	0.61 ± 0.1	4.6 ± 0.4	15.0 ± 2.0	
0.6	2.2 ± 0.4	11.0 ± 1.5		
0.8	2.2 ± 0.4[4]	11.8 ± 0.6[3]	45.0 ± 10.0[1]	
1.8	7.2 ± 1.0	35.0 ± 2.5		

Unless marked with a (1) all data presented were observed during August and September 1966.

1) Observations made in 1967.

2) 1.7 ± 0.2 was measured in Aug. 1967.

3) 11.0 ± 2.0 was measured in May 1967.

4) 2.8 ± 0.6 was measured in May 1967.

Figure 11

The infrared spectrum of the radiation from an area centered on the position of maximum brightness and 3.5 arc min in diameter is shown. The 10 μ limit was obtained by Hughes (17). The radio spectrum of Sagittarius A (3) is also included as well as the infrared spectrum of the nucleus of M 31 (19, 21). The spectrum of M 31 is normalized to an arbitrary energy scale.

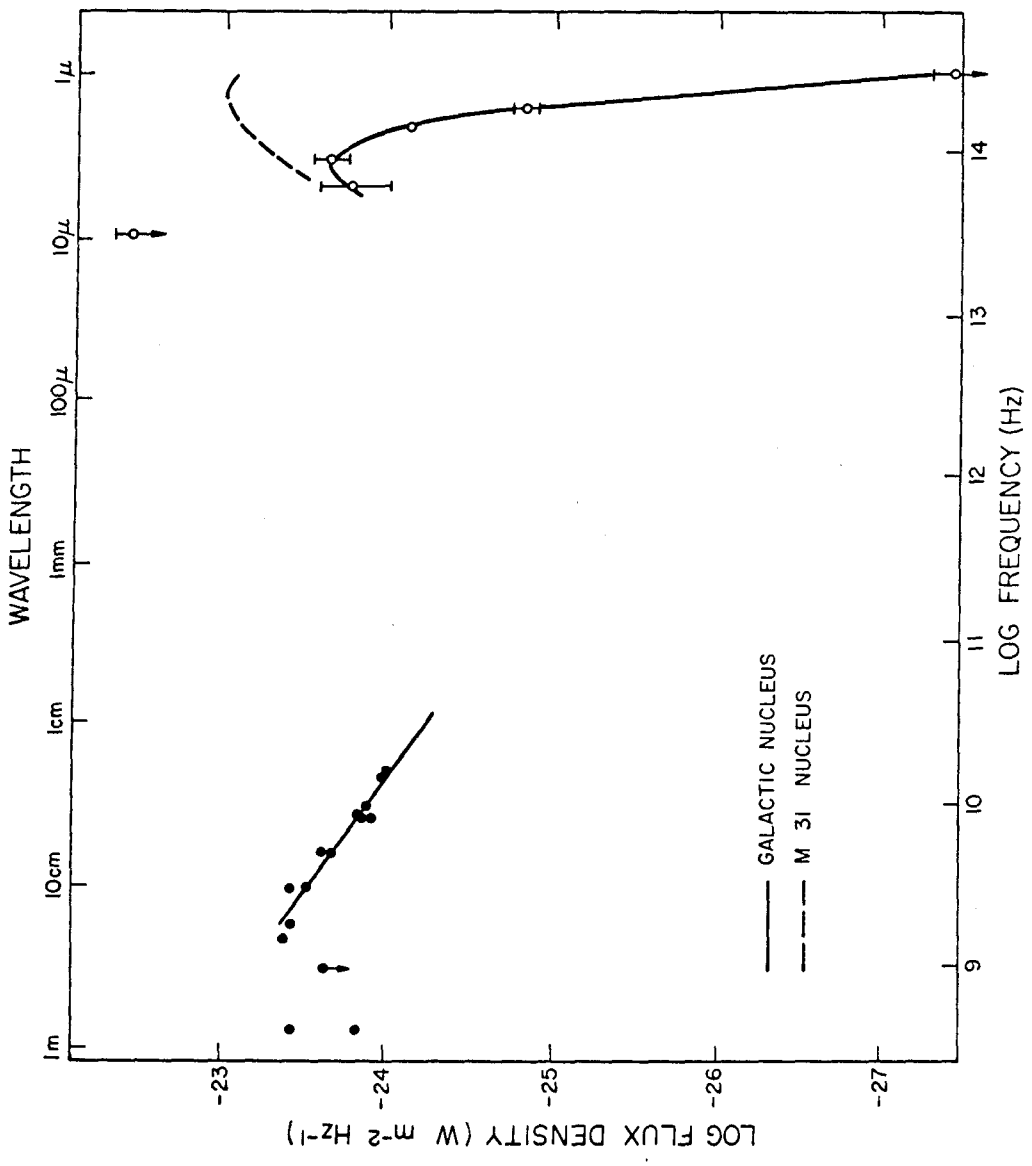
WAVELENGTH
1m
10cm
1cm
1mm
100μ
10μ
1μ
LOG FLUX DENSITY (W m⁻² Hz⁻¹)
-23
-24
-25
-26
-27
LOG FREQUENCY (Hz)
9
10
11
12
13
14
GALACTIC NUCLEUS
M 31 NUCLEUS

Figure 11

while the 1.65 and 0.9 μ points were found from Table 5 using the data within 3.5 arc min diameter of the position of maximum brightness. The 3.4 and 4.8 μ points were extrapolated from the data shown in Table 6 with the assumption that the color is constant over the 3.5 arc min area. From the color ratios, $B_\nu(1.65)/B_\nu(2.2)$, measured over the entire region (Tables 5 and 6) this assumption appears valid, especially at 3.4 μ where reliable data extend out to 0.8 arc min diameter. Data at radio wavelengths (3) and a 10 μ upper limit measured by Hughes (17) using the 62-inch infrared sky survey telescope on Mt. Wilson have also been included in the figure.

There are several uncertainties which enter into the quoted flux densities and surface brightnesses. The most basic uncertainty comes from the noise in the detector and from noise produced by fluctuations in the background radiation. This error is easy to determine from the noise on the strip chart recorder. The second uncertainty comes from changes in the relative sensitivity due to time variations in the response of the system and time variations in the transparency of the atmosphere. From the scatter in the deflections of standard stars it has been found that on the average the sensitivity is known to about $\pm$ 8% at 1.65 and 2.2 μ, $\pm$ 12% at 3.4 μ, and $\pm$ 20% at 4.8 μ. Another error which enters into the surface brightnesses quoted, is the uncertainty in the area of the apertures used for the observations; from the response profiles of standard stars this error has been estimated to be $\pm$ 5%. All of the errors and uncertainties mentioned above have been included in the presentation of the data.

There is one other known error which has not been included in the data presented. This error is the 5 to 10% uncertainty in the absolute calibration discussed in Appendix A. If a calculation is made using the data presented in this section the possible uncertainty in the calibration must also be considered.

V. SUMMARY OF DATA

A. Description

Radiation from the galactic center region at 2.2 μ can conveniently be discussed in five parts:

i) A dominant source which agrees in position and extent with the radio source Sagittarius A.

ii) A point-like source of radiation located within the dominant source (i) and near the position of its maximum brightness.

iii) A general background radiation distributed predominantly along the galactic plane.

iv) Several smaller extended sources.

v) A distribution of point-like sources scattered over the galactic center region.

(i). The dominant source, which is approximately in the center of Fig. 8, has a full width at half maximum of 3 to 5 arc min when observed with 1.8 arc min resolution (Fig. 4), and has a total extent of 5 to 10 arc min diameter. There is both a definite elongation and an asymmetry along the galactic plane at 2.2 μ. The axial ratio is approximately 2:1 in all three contour maps (Figs. 8, 9, 10). The region 3-5 arc min northeast of the source center is twice as bright as a similar region southwest of the center when viewed with 1.8 arc min resolution (see Fig. 8); however, the very central region of the source within a diameter of 5 arc min does not show this asymmetry (see Figs. 9 and 10). Across the galactic plane there also appears a noticable

asymmetry. The southeast edge of the source is much steeper than the corresponding northwest edge (see Figs. 4, 7b, 8 and 9).

The flux densities at 2.2 μ observed with different sized circular apertures centered on the point of maximum brightness are plotted in Fig. 12. For diameters greater than 1.8 arc min it was necessary to integrate the data of Figs. 8 and 9 numerically; in all cases the energy contained in the point-like source (ii) was subtracted. It is seen that the spatial distribution is non-Gaussian but approximately follows a power law such that the flux density within a circular area of diameter D is proportional to $D^{1.2\pm0.1}$ corresponding to a mean surfact brightness which is proportional to $D^{-0.8\pm0.1}$.

The power law described above is valid for almost the entire range of the dominant source. At 0.08 arc min resolution (Fig. 5) there is evidence that the distribution of flux density departs from the power law dependence and flattens into a core of radiation with a full width at half maximum of approximately 0.3 arc min. The evidence for this core is given in Fig. 13 where two observed scans are compared with two scans derived under the assumption that the brightness distribution has the form $B \propto D^{-0.8}$. The derived curves shown have been normalized to agree with the aperture diameters and maximum deflections shown in Figs. 4 and 5. For 1.8 arc min resolution (Fig. 4) the observed and derived traces agree very well, confirming the power law behavior in the region $D \sim 2$ arc min. For 0.08 arc min resolution (Fig. 5) the obsserved trace is considerably wider than the derived traces, indicating a departure from the power law behavior in the region $D \sim 0.1$ arc min. Although the surface brightness of the central

Figure 12

The flux density at 2.2 μ as observed with apertures centered on the position of maximum brightness is shown. The energy of the point-like source (ii) has been subtracted.

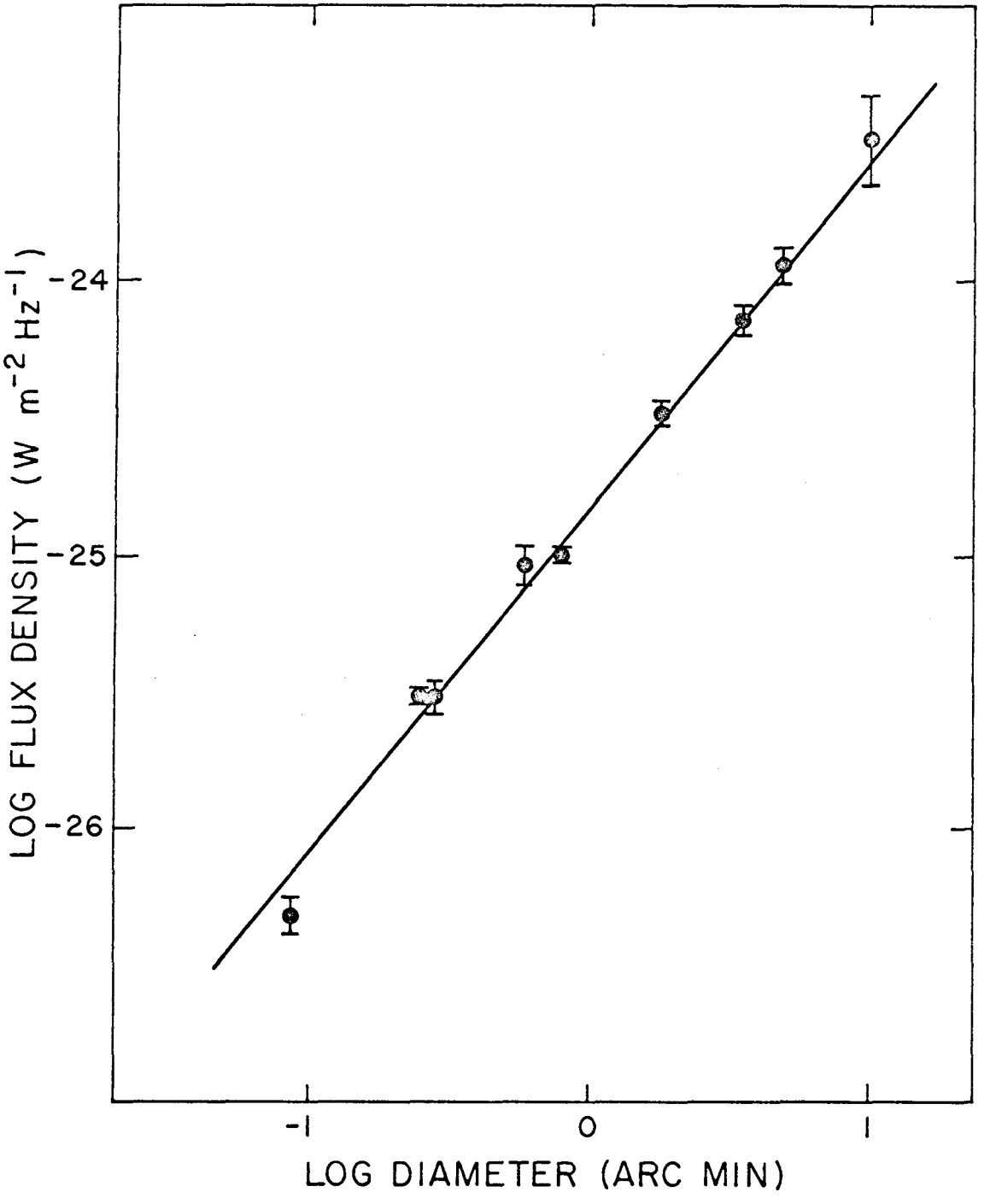

Figure 12

Figure 13

A comparison is made between two observed scans and two scans which have been theoretically derived. Place Fig. 13a and Fig. 13b together with a light behind them to make the comparison.

Figure 13a

Shown is the convolution of a circular aperture with the two dimensional brightness distribution $B(D) \propto D^{-0.8}$. The top trace has been normalized to the aperture diameter and maximum deflection shown in Fig. 4 (1.8 arc min resolution); the bottom trace has been normalized to the aperture diameter and maximum deflection shown in Fig. 5 (0.08 arc min resolution). The effects of the system time constant and atmospheric seeing have been neglected. [For 0.08 arc min resolution (Fig. 5) the effects of atmospheric seeing could not increase the width of the derived trace by more than 20% since the average width of the response function is only 20% smaller than the maximum width.]

Figure 13b

Shown are two telescope scans. The top trace is the same as the scan in Fig. 4 (1.8 arc min resolution); the bottom trace is the same as the lower left scan in Fig. 5 (0.08 arc min resolution).

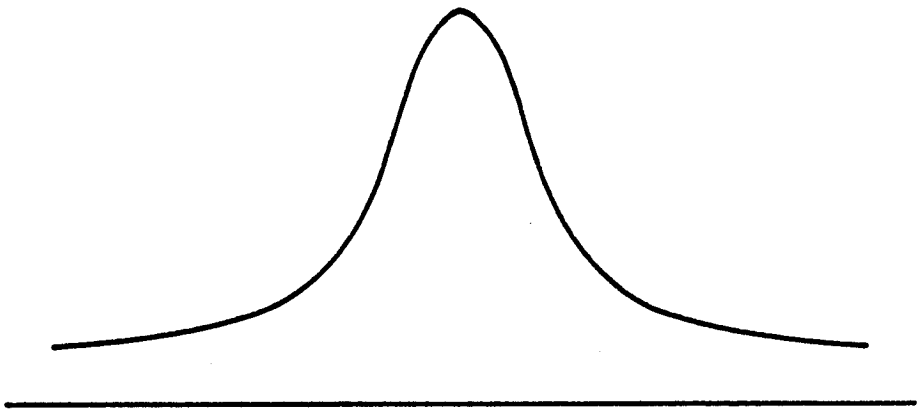

Derived Trace Corresponding to 1.8 arc min Resolution

Derived Trace Corresponding to 0.08 arc min Resolution

Figure 13a

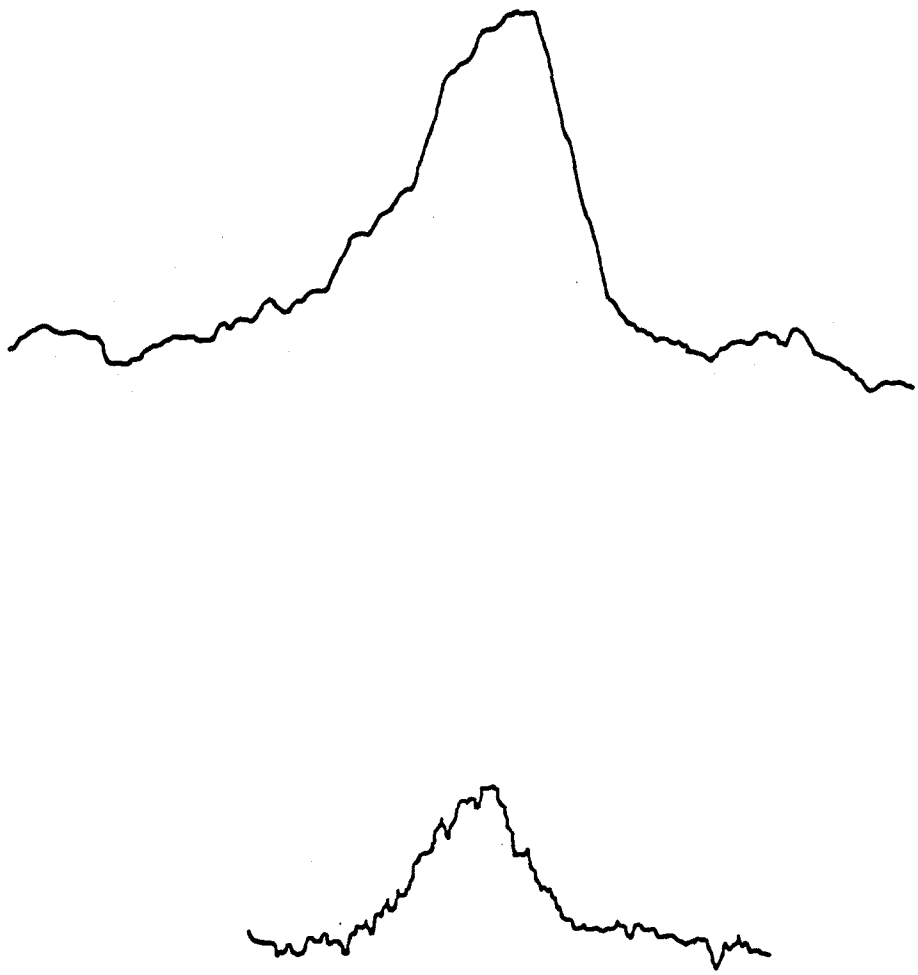

Figure 13b

core 0.3 arc min in diameter is larger than that of the surroundings, the total flux density in the core at 2.2 μ is about 4% of the total flux density in the dominant source (i). The determination of the largest diameter for which the power law holds is complicated by secondary sources and the low surface brightness of the dominant source away from its center.

The color ratio $B_\nu(1.65)/B_\nu(2.2)$ is almost constant over the dominant source with a mean value of 0.20 ± 0.03. In Appendix B there is some evidence that the edges of the source, 3-5 arc min from the center, are bluer than the central region. (In particular the bright region 3-5 arc min northeast of the center has a color ratio $B_\nu(1.65)/B_\nu(2.2) = 0.30 \pm 0.05$.) Within the central 0.8 arc min the color ratio $B_\nu(3.4)/B_\nu(2.2) = 3.3 \pm 0.5$ while $B_\nu(0.9)/B_\nu(2.2)$ is less than 0.001. The observed energy distribution is similar to that of a 900° K black body.

(ii). Figure 5 shows a point-like source displaced 10 arc sec from the centroid of the bright core of radiation. At 2.2 μ this source has a diameter less than 2 arc sec, a K-magnitude of 6.7, and a flux density of 1.4×10^{-26} W m^{-2} Hz^{-1}. Over a one-year period the 2.2 μ flux density was constant to within the errors (see Table 6). The color ratios $B_\nu(1.65)/B_\nu(2.2)$ and $B_\nu(3.4)/B_\nu(2.2)$ of this source are 0.15 ± 0.03, and 3.2 ± 0.6. These color ratios agree within the errors to the average color ratios of the dominant source (i).

(iii). The general background radiation is best seen in Fig. 8. The extent and brightness of the background is not well

determined, although it appears that it may be an extension of the dominant source. The total flux density in the background is approximately 10^{-23} W m^{-2} Hz^{-1} at 2.2 μ over the area 40 arc min in diameter surrounding the source, but is subject to large uncertainties since the level of zero flux is unknown.

(iv). Figure 8 shows seven additional localized sources of radiation whose approximate central coordinates are listed in Table 7. The 2.2 μ flux density of each secondary source is about one-fifth that measured from the dominant source; in addition, it is pointed out in Appendix B that the maximum 2.2 μ surface brightness of each secondary source is at least five times fainter than the maximum surface brightness of the dominant source (i), when observed with 0.8 arc min resolution.

Sources B, C, D and G all have a color ratio $B_\nu(1.65)/B_\nu(2.2)$ approximately three times larger than the dominant source (Table 5 and Table 4B of Appendix B). In Appendix B it is shown that the surface density of secondary extended sources decreases rapidly as one moves away from the galactic center; within a radius of 15 arc min of the center the density is larger than 10^{-2} per square arc min while 15 to 50 arc min away the density is less than 10^{-3} per square arc min.

(v). Data on point-like sources distributed over the galactic center region are discussed in Appendix B. The point sources have been studied down to a 2.2 μ flux density of 1.6×10^{-26} W m^{-1} Hz^{-1} ($K \simeq 6.5$). The surface density of these sources has a fairly uniform value of $3 \pm 1 \times 10^{-2}$ per square arc min over a region 2 degrees in

TABLE 7

COORDINATES OF SECONDARY SOURCES

Designation	Declination (1950)	Right Ascension (1950)
A	$-28^{\circ}\ 42'$	$17^{h}\ 42.3^{m}$
B	$-28^{\circ}\ 57'$	$17^{h}\ 44.0^{m}$
C	$-29^{\circ}\ 00'$	$17^{h}\ 41.9^{m}$
D	$-29^{\circ}\ 00'$	$17^{h}\ 42.7^{m}$
E	$-29^{\circ}\ 02'$	$17^{h}\ 43.1^{m}$
F	$-29^{\circ}\ 10'$	$17^{h}\ 41.9^{m}$
G	$-29^{\circ}\ 11'$	$17^{h}\ 41.0^{m}$

diameter centered on the galactic center. It appears that the surface density of the sources in the plane of the sky does not increase as one moves in toward the galactic center. The value of the average color ratio $B_\nu(1.65)/B_\nu(2.2)$ for these sources is 0.9 ± 0.4. The total 2.2 μ flux density measured from these sources in an area 40 arc min in diameter centered on the dominant source is 1.5×10^{-24} W m^{-2} Hz^{-1}.

B. Comparison with Dynamical Center

The coordinates of the dynamical center of the Galaxy have been measured by Oort and Rougoor (1) to be:

Right Ascension (1950)	$17^h\ 42.7^m \pm 0.4^m$
Declination (1950)	$-28^\circ\ 56'\ \pm\ 5'$

As seen from Fig. 8, these coordinates lie within 4 arc min of the position of maximum brightness of the dominant source.

C. Comparison of Infrared and Radio Observations

Radio observations of the center of the Galaxy (3) show:
(a) a bright discrete source 3 to 4 arc min in diameter--Sagittarius A,
(b) several weaker secondary sources a few arc min in diameter, and
(c) an extended background about one degree in diameter.

The dominant infrared source (i) agrees in position with Sagittarius A; the 1950 coordinates of the position of maximum infrared brightness with 0.25 arc min resolution and the mean position of Sagittarius A (3) are:

	Right Ascension	Declination
Radio	$17^h\ 42^m\ 28^s \pm 2^s$	$-28^\circ\ 58.5' \pm 0.5'$
Infrared	$17^h\ 42^m\ 30^s \pm 1^s$	$-28^\circ\ 59.5' \pm 0.1'$[1]

When observed with 1.8 arc min resolution, the dominant source has a full width at half maximum of 3-5 arc min, which agrees with the width measured by Downes, Maxwell, and Meeks (18) at 1.9 cm using 2.2 arc min resolution (Fig. 14). Also, both the infrared and radio maps show an elongation along the galactic plane, with the region 5 arc min northeast of the center being brighter than a similar region southwest of the center. Radio observations with pencil beam resolutions finer than 2 arc min have not been published, so a comparison of the fine structure within the source cannot be made. The agreement in the positions and sizes of the radio source Sagittarius A and the dominant infrared source strongly suggests that the two sources are spatially coincident.

An extrapolation of the radio flux density into the infrared predicts a 3.4 μ flux density a factor of 10^3 less than that observed (Fig. 11); therefore the infrared radiation is not a simple extension of the non-thermal source Sagittarius A, and a further discussion on the possible mechanisms for generating the infrared radiation is required.

---

[1] The errors quoted represent the statistical deviations of four independent measurements taken on three different nights and at four different air masses. Three of the measurements were made with respect to the star γ Sgr., while one measurement was made with respect to both γ Sgr. and ϕ Sgr.

Figure 14

A contour map of the galactic center region at 1.9 cm is shown from Downes, Maxwell, and Meeks (18). Contours represent antenna temperature in °K. The coordinate scale is the same as Fig. 8.

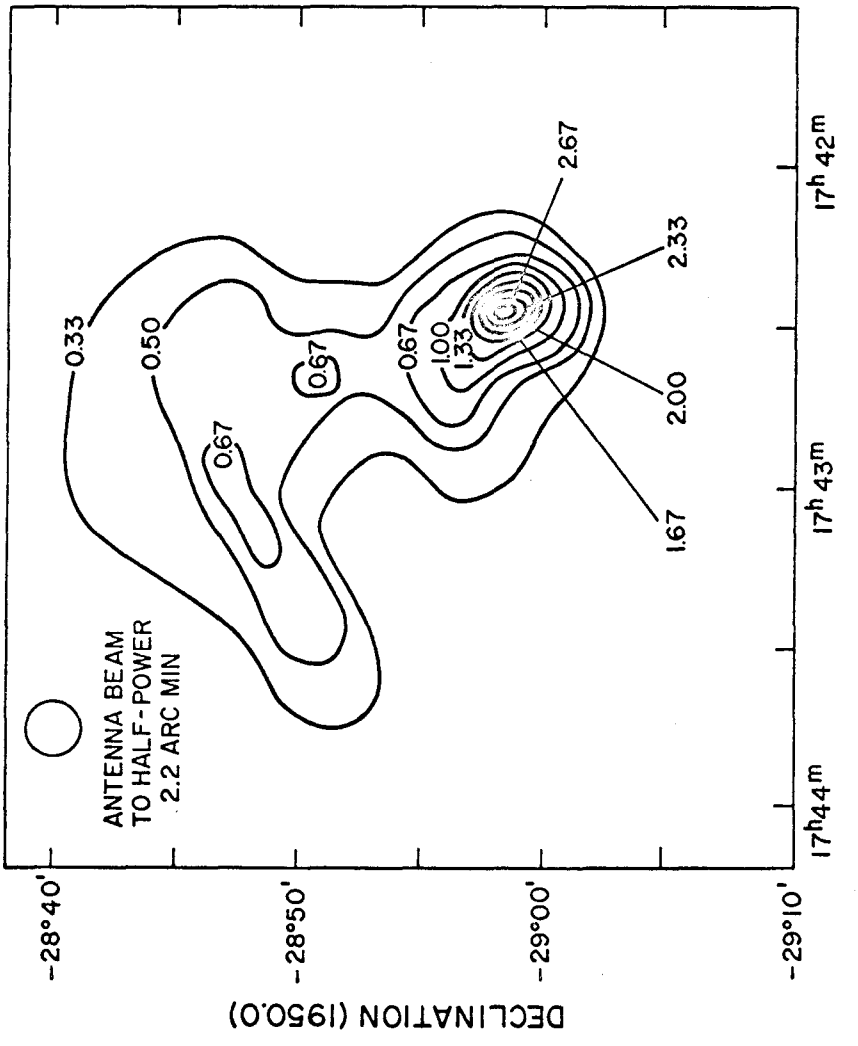
0.33
0.50
0.67
0.67
0.67
1.00
1.33
2.67
2.33
2.00
1.67
ANTENNA BEAM
TO HALF-POWER
2.2 ARC MIN
-28°40'
-28°50'
-29°00'
-29°10'
17h44m
17h43m
17h42m
DECLINATION (1950.0)
RIGHT ASCENSION (1950.0)

Figure 14

Except for the dominant infrared source (i) there seems to be little correlation between the localized radio and infrared sources. However, good infrared scans have been made over only a few of the radio sources in the galactic center region.

The data on the infrared background radiation are not sufficient to make a definitive comparison with the radio background. However, both are concentrated along the galactic plane, and extend about 1/2 degree from the dominant source.

D. Comparison with M 31

Profiles at 2.2 μ of the galactic center and of the nuclear region of M 31 observed by Neugebauer and Becklin (19) are shown in Fig. 15. For the galactic center the instrumental resolution was degraded from the data presented in Fig. 8 by numerically averaging over the appropriate area so that the two profiles would have the same resolution of 14 pc [r(M 31) = 570 kpc; (20)]. At 3.4 μ, where interstellar absorption is low, the observed mean surface brightness of M 31 measured by Johnson (21) agrees within a factor of two with the extrapolated mean surface brightness of a similar area of the galactic center. The extrapolation was made under the assumption that the intrinsic color of the source is constant over the region in question; measurements at 2.2 and 1.65 μ by Neugebauer and Becklin (19) show that this is correct for the nucleus of M 31.

Figure 15

A right ascension scan of M 31 at 2.2 μ (19) is compared with a 2.2 μ scan of the center of the Galaxy. The latter was taken from the data of Fig. 8 along a line 50° to the galactic plane with a resolution degraded to correspond to the observations of M 31.

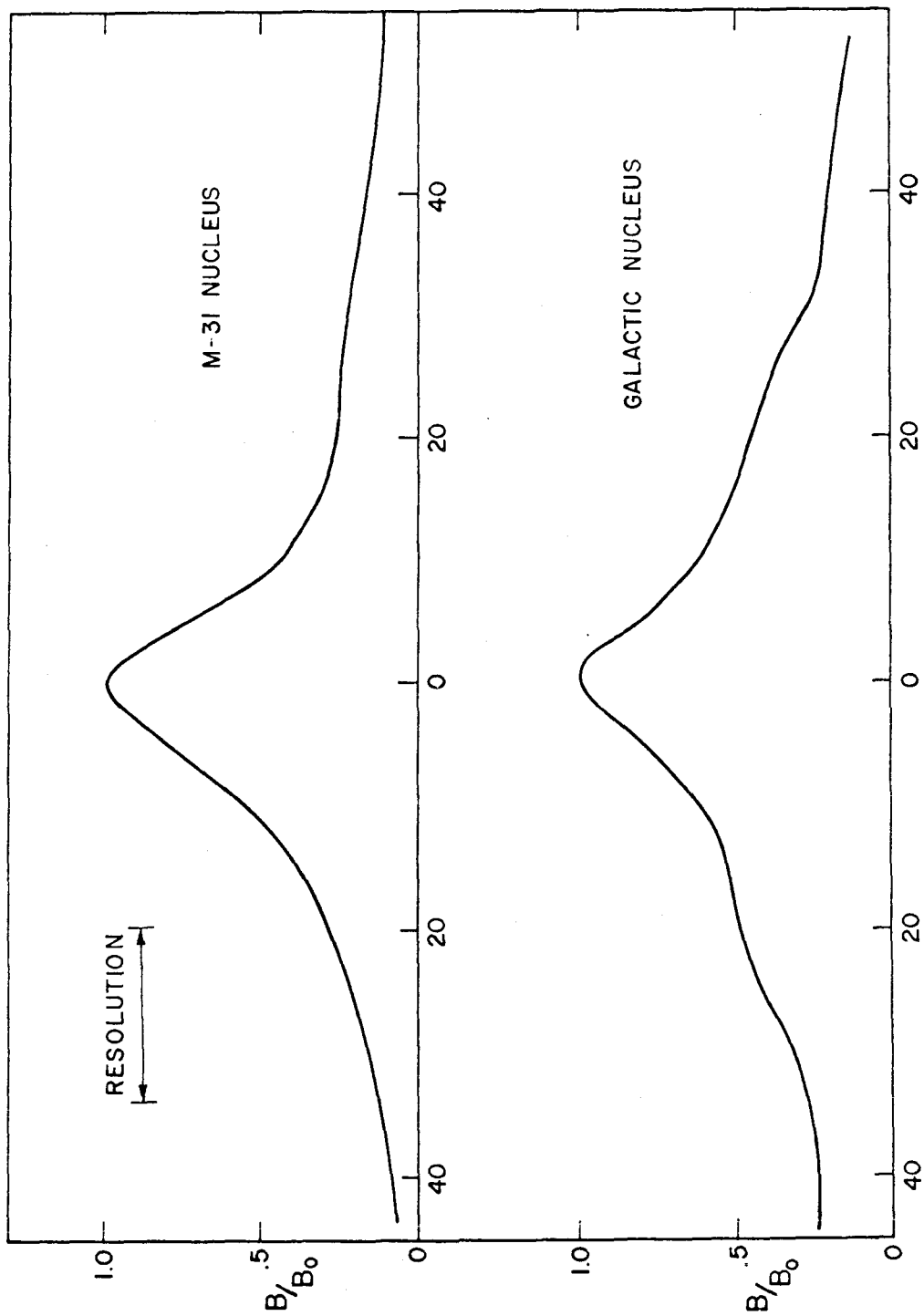
M-31 NUCLEUS
GALACTIC NUCLEUS
RESOLUTION
B/B₀
1.0
.5
0
40
20
0
20
40
DISTANCE (pc)

Figure 15

VI. DISCUSSION

We now consider the nature of the source of the infrared radiation from the galactic center. In the first four sections we shall assume that the infrared radiation is of stellar origin and that the observed 900° K black body spectrum arises from the effects of interstellar absorption upon the spectra of ordinary stars. In Section E we discuss the possibility that the source of the infrared radiation is non-stellar. The "point" source seen in Fig. 5 will be considered after the extended sources are discussed.

A. Interstellar Absorption

The energy spectrum observed in the dominant infrared source is a function of both the emitted energy spectrum and the total amount and spectral characteristics of the interstellar absorption. In this section, the intrinsic color of the galactic center and the interstellar reddening curve are assumed known; the total amount of obscuration and the infrared energy emitted by the source are then calculated.

For calculations made in the next four sections the intrinsic energy spectrum of the galactic center region is assumed to be that measured in the nucleus of M 31 by Johnson (21) and by Neugebauer and Becklin (19); as shown in Fig. 11, it approximates a 4000° K black body. The infrared interstellar absorption law is averaged from the results of Johnson and Borgman (22) and Johnson (23) for the solar neighborhood in the direction of the galactic center; this average, which is shown in Table 8, agrees with the observations of Whitford (12)

TABLE 8

EXTINCTION COEFFICIENTS

$\lambda(\mu)$	A
0.55	1.00
0.90	0.46
1.25	0.30
1.65	0.17
2.2	0.10
3.4	0.045
4.8	0.02

and calculations by van de Hulst (24) for dielectric grains (Curve No. 15).

The total absorption is found from the equation

$$\left(B_{\nu 1}/B_{\nu 2}\right)_{obs} = \left(B_{\nu 1}/B_{\nu 2}\right)_{emit} \exp\left(-\tau_o(A_1 - A_2)\right) \qquad (1)$$

where $B_{\nu 1}$ is the surface brightness (W m^{-2} Hz^{-1} $ster^{-1}$) at $\nu 1$, A_1 is the extinction coefficient at $\nu 1$ normalized to 1.00 at 0.55 μ (Table 8), and τ_o is the total optical depth at 0.55 μ. Using the observed color ratios discussed in the previous sections and the intrinsic color ratios which have been measured in the nucleus of M 31 (at 3.4 and 4.8 μ the colors of a 4000° K black body were used) the following values of τ_o were calculated:

Color Ratio	Observed	Intrinsic	τ_o
$B_\nu(1.65)/B_\nu(2.2)$	0.20 ± 0.03	1.2 ± 0.1	25 ± 4
$B_\nu(3.4)/B_\nu(2.2)$	3.2 ± 0.5	0.6 ± 0.1	30 ± 10
$B_\nu(4.8)/B_\nu(2.2)$	2.5 ± 1.3	0.4 ± 0.1	23 ± 8
$B_\nu(0.9)/B_\nu(2.2)$	< 0.001	1.0 ± 0.1	> 20

The errors shown for τ_o mainly reflect the estimated uncertainty in the reddening law.

The agreement of all four values gives confidence that the initial assumptions about the absorption law and the intrinsic energy spectrum are correct.[2] The value $\tau_o = 25$ will be adopted for further calculations.

---

[2] The intrinsic energy distribution used was similar to a 4000° K black body; however, any black body distribution with T > 3000° K will give essentially the same results.

Further confidence in the assumptions is provided by the calculation that the mean intrinsic surface brightness of the galactic center at 2.2 μ out to a diameter of 14 pc is 10^{-17} W m^{-2} Hz^{-1} $ster^{-1}$[3] while a comparable quantity for M 31 is 0.4×10^{-17} W m^{-2} Hz^{-1} $ster^{-1}$[4]. In comparison, the mass of the galactic nucleus as determined by Rougoor and Oort (25) and the mass of the nucleus of M 31 as determined by Kinman (26) from the data of Lallemand, Duchesne, and Walker (10) agree within a factor of three.

The total calculated absorption in magnitudes and the ratio of measured to emitted brightness are given as a function of wavelength in Table 9. The total visual absorption of the galactic center of 27 magnitudes is in good agreement with the results of Neckel (28) for the region within 0.5 kpc of the Sun. Using early stars with known MKK spectral types and photoelectrically determined magnitudes, Neckel finds that the average visual interstellar absorption in the galactic plane is 2.46 mag kpc^{-1}. The agreement of the two numbers suggests the average dust density between the Sun and the galactic center is similar to the dust density in the local solar neighborhood.

The absorption curve used above included no wavelength independent absorption although Moroz (11) explained his failure to detect radiation as most probably caused by the existence of one or two magnitudes of neutral absorption. If this amount of neutral absorption were

---

[3]From Fig. 12 the measured flux density is 1.2×10^{-24} W m^{-2} Hz^{-1}, from Table 9 the absorption causes a reduction of a factor of 12, and the 14 pc core covers a solid angle of 1.5×10^{-6} $ster^{-1}$.

[4]The measured flux density is 1.8×10^{-27} W m^{-2} Hz^{-1} (19) and the 14 pc covers a solid angle of 4.5×10^{-10} $ster^{-1}$.

TABLE 9

CALCULATED ABSORPTION TO THE GALACTIC CENTER

$\lambda(\mu)$	ΔM	$(B_\nu)_{obs}/(B_\nu)_{emitted}$
0.55	27.0	10^{-11}
0.90	13.0	10^{-5}
1.65	4.6	0.02
2.2	2.7	0.1
3.4	1.2	0.3

present, then at 2.2 μ the galactic center would be intrinsically about 10 times brighter than a similar region of M 31.

For selected areas of the sky, Johnson (23, 29) has derived a reddening curve which, for wavelengths less than 3 μ, has a much larger extinction coefficient than shown in Table 8. If the reddening of the galactic center radiation were given by the simple average of the extinction curves recently summarized by Johnson (29) (Figs. 24-37), then the galactic nucleus would be intrinsically 75 times brighter than the nucleus of M 31. Both Moroz's and Johnson's extinction curves result in a luminosity for the galactic center which is inconsistent with the mass determinations of the galactic center and the nucleus of M 31.

In summary, if the luminosities of the nucleus of M 31 and of the galactic nucleus are equal within a factor of three and both nuclei have similar colors, then the interstellar reddening curve extrapolates to $1/\lambda \rightarrow 0$ in a manner shown in Table 8 and the extinction coefficient at 2.2 μ cannot be greater than 15 percent of the visual extinction coefficient. For example, if $\tau_o = 25$ and the galactic center is three times brighter than a similar region of M 31, the ratio of the 2.2 to 0.55 μ extinction coefficients is 0.12, while if the nucleus of M 31 is three times brighter than a similar region of the galactic center then the same ratio os 0.03.

B. Secondary Extended Sources

If the infrared radiation of the dominant source is of stellar origin, it is important to ask whether the secondary sources are extensions of the central source viewed through relatively little obscuration or whether they are separate clusters of stars.

Evidence that the secondary sources could be extensions of the central source comes from their observed relatively blue colors (Table 5) and their brightnesses. When the brightnesses of the secondary sources are corrected, using an optical depth derived purely from the observed colors, the secondary sources no longer stand conspicuously above the background. Unfortunately, the uncertainties in the background levels are too large to make the conclusion quantitative.

The sources could be discrete star clouds, in which case the observed blue colors imply they are probably between the Sun and the galactic center.[5] Since the sources are highly concentrated in the galactic center region (Appendix B) the close angular separations between the center of the Galaxy and the secondary sources indicate that these sources are in fact separated by about 100 pc. Therefore, to satisfy the observed colors, 10 to 15 magnitudes of visual absorption must exist in the central region of the galactic center. However, extragalactic systems do not exhibit such a dense concentration of absorbing material towards their nuclear regions (5). The true nature of the secondary sources can only be found from further observational data.

C. Uniformly Distributed Point Sources

The uniformly distributed "point-like" sources found in the galactic center region probably have no physical connection with the

---

[5] This conclusion is reached only when it is assumed that the blue colors are caused by a lack of interstellar reddening rather than by intrinsic properties of the source. This assumption is probably correct, because if equal amounts of absorption exist for both the dominant and secondary sources, and the dominant source is of a stellar origin, then the intrinsic energy distribution of the secondary sources decreases at long wavelengths more rapidly than an infinite temperature black body.

galactic nucleus. This follows from three observational properties of the point sources discussed in Appendix B:

a) There is no tendency for the surface number density of the point-like sources to increase as one moves in toward the galactic center.

b) The measured surface density of the sources is consistent with the average density expected from extrapolation of the sources found on the California Institute of Technology infrared sky survey in the region $|b^{II}| < 2.5°$, $0° < \ell^{II} < 90°$.

c) The colors of these sources are considerably bluer than the colors of the extended sources of radiation.

The measured surface number density of the sources is consistent with the hypothesis that most of the radiation is produced in M giant stars 1 - 5 kpc from the Sun (30). The average visual absorption shown by these stars is calculated to be about 4 magnitudes (see Appendix B).

D. Physical Properties of the Galactic Center

Some inferences about the physical nature of the galactic center can be made using the results of the previous sections. The 2.2 μ intrinsic brightnesses of the dominant source averaged over circular areas centered on the position of maximum brightness have been calculated from the derived optical depths (Table 9). In addition, the total luminosities have been estimated assuming an energy distribution equal to that measured by Johnson (21) for the nuclear region of M 31. The results of these calculations are presented in Table 10 as a function of diameter; the uncertainty in the interstellar reddening curve introduces approximately a factor of 2 uncertainty in these results.

TABLE 10

CALCULATED INTRINSIC PHYSICAL PROPERTIES

Diameter (pc)	Mean Intrinsic 2.2 μ Surface Brightness (10^{-18} W m^{-2} Hz^{-1} $ster^{-1}$)	Intrinsic Luminosity (10^6 $L_\odot$)*	Mass (10^6 $M_\odot$)+
1	78	1	3
2	45	2	6
5	21	7	20
10	12	15	45
20	7	35	100
40	4	80	230
60	3	130	370

*$L_\odot = 4 \times 10^{26}$ watts.

+$M_\odot = 2 \times 10^{30}$ kgrams.

The total mass can be found from the calculated luminosity if a mass to luminosity ratio for the stars in the galactic center is estimated. For M 31, the following values of M/L_{pg} have been determined: 23 by Schmidt (31), 16 by Spinrad (32), and 3.6 by Lallemand, Duchesne, and Walker (10). Schmidt's (31) determination is for the whole of M 31, while the others are for the nuclear region only. The total mass producing the observed radiation within a circular area is given in Table 10 for $M/L_{ph} = 10$; since the surface brightness increases rapidly toward the center, the observed mass within a given projected diameter is effectively equal to the mass within a sphere of the same diameter.[6] The mean density in the 1 pc diameter central core is approximately 10^7 times the density in the neighborhood of the Sun. The power law dependence of the flux density, as shown in Fig. 8, implies that the mass density of material falls from the center approximately as $R^{-1.8}$.

Rougoor and Oort (25) have determined the mass within 70 pc of the galactic center and have estimated, by extrapolation, that the mass within a radius of 20 pc is 0.7×10^8 $M_\odot$. According to Table 10, the mass inside a radius of 20 pc is 2.3×10^8 $M_\odot$; this agreement gives added confidence in the assumptions.

The high stellar density obtained for the bright 1 pc diameter core suggests that stellar collisions should be considered. Using a

---

[6] For the idealized case where the mass density falls off from the center as R^{-2}, the mass within a spherical volume of a given radius is 64% of the observed mass within a cylinder of the same radius. Numerical integrations for a $R^{-1.8}$ law show a ratio of about 55%, however since the problem is complicated further by the fact that the quoted numbers are not absolute, but rather a comparison of two positions in the sky, no correction has been applied.

model of Spitzer and Saslaw (33) for the collision rates of stars, the average length of time before a star of one solar mass is involved in a physical collision is about 10^{10} years in the 1 pc diameter core, if the mass of the core is equal to 3×10^{6} $M_{\odot}$. The collisional rate would be about 10^{-4} yr^{-1}, however, Spitzer and Saslaw (33) have considered the effects of such collisions and find that for the small rms velocities expected ($\sim$ 100 km/sec) negligible amounts of gas and energy would be released.

E. Other Models for the Galactic Center

Although the assumption that the observed infrared radiation arises from a stellar population similar to that present in the nuclear region of M 31 is consistent with the data, other models for the source of radiation which cannot be completely ruled out at present will be considered. In fact, the possibility that the origin of the infrared radiation from the center of the Galaxy is not the same as the origin in the nucleus of M 31 is increased by the recent radio observations of Pooley and Kenderdine (27) which indicate that the nuclear region of M 31 does not have a counterpart to Sagittarius A. An upper limit to the 21 cm continuum of a possible source in the nucleus of M 31 is 1/20 the brightness of Sagittarius A.

Part of the infrared radiation could originate from a non-thermal source at the center of the Galaxy. In fact, if 15 magnitudes of visual absorption are assumed between the sun and the galactic center, the corrected spectral energy distribution of the galactic center has

features strikingly similar to those of the measured energy distribution of NGG 1068 (Fig. 16) (34, 35, 36). The energy distribution of 3C 273 also has qualitatively similar features (37).

The source of non-thermal radiation which is discussed most often is the synchrotron mechanism. In this section the possibility will be considered that the infrared and radio spectral distribution shown in Fig. 16 results from a distribution of relativistic electrons in a magnetic field.[7] The electron energy distribution needed to produce the radio radiation is discussed by Downes and Maxwell (3). They find that a distribution of electrons of the form $N(E) \propto E^{-2.4}$ will produce the observed radio radiation between 2 and 20 cm (observations at wavelengths longer than 20 cm are effected by absorption from an ionized gas). However, an electron distribution of this form produces only negligible infrared radiation (with the above electron distribution a straight line extrapolation of the radio data can be used to predict the infrared radiation). The additional electron energy distribution needed to produce the infrared radiation can be obtained from the synchrotron equations (41). If a relativistic electron of energy E (ergs) is in a magnetic field of strength H (gauss) then it radiates spectrally at the average rate

---

[7] The possibility that the flux density distribution is a result of absorption (for example synchrotron self absorption, absorption by an ionized gas, or absorption by interstellar grains) or the Razin effect seems unlikely, since the observation would require a suppression of the radiation only in the selected region 10 to 1000 μ. Such localized absorption or suppression is not theoretically predicted.

Figure 16

The spectral energy distribution of the galactic center corrected for 15 magnitudes of visual absorption is compared to the energy distribution observed in NGC 1068 (34, 35, 36). The dashed curve is the spectral energy distribution expected from a synchrotron source with monoenergetic electrons which have $\nu_c = 10^{14}$ Hz. The curve has been normalized to agree with the galactic center datum point at 10^{14} Hz.

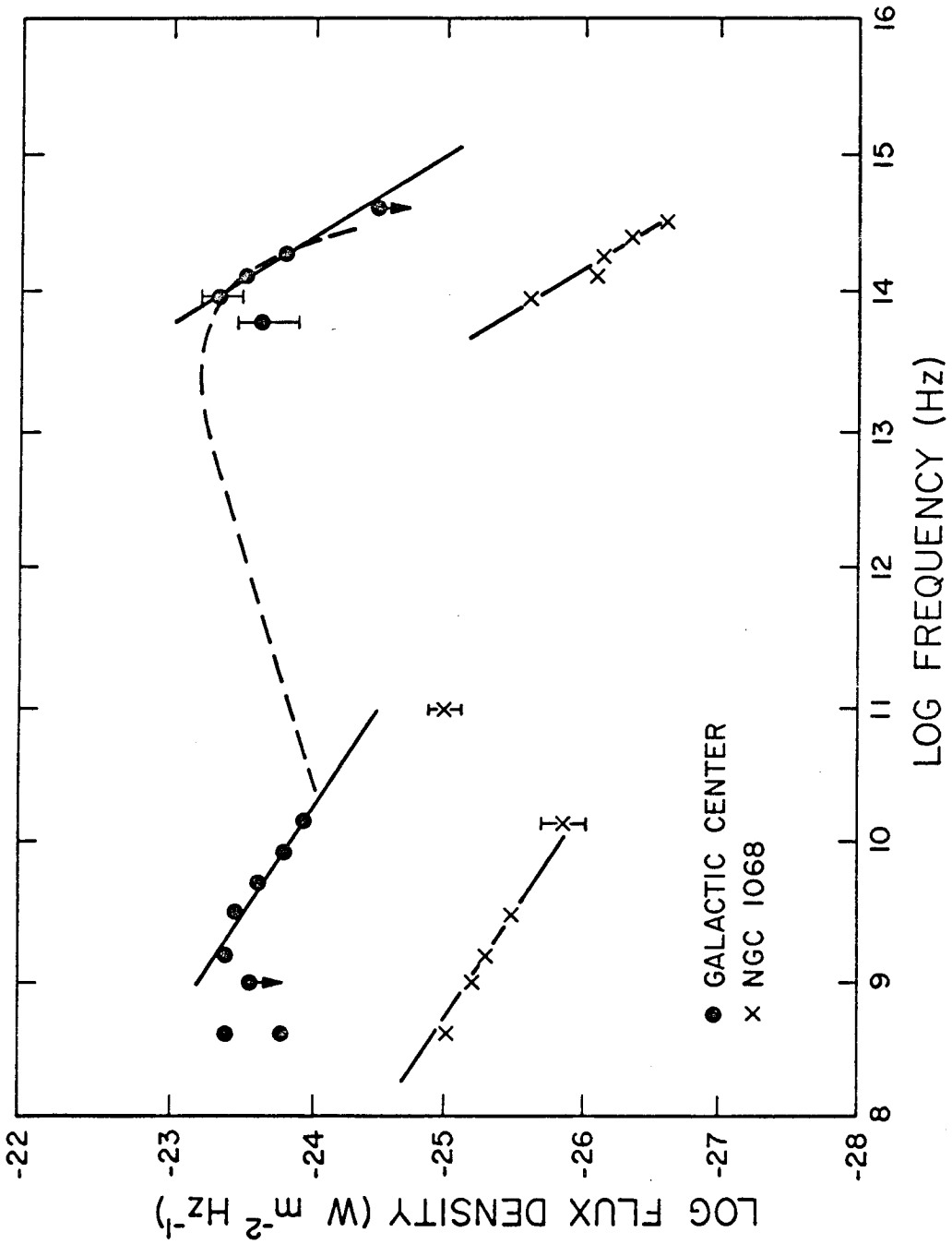
LOG FLUX DENSITY (W m⁻² Hz⁻¹)
-22
-23
-24
-25
-26
-27
-28
8
9
10
11
12
13
14
15
16
LOG FREQUENCY (Hz)
● GALACTIC CENTER
× NGC 1068

Figure 16

$$P(\nu) = 2.34 \times 10^{-22} H_{\perp} (\nu/\nu_c) \int_{\nu/\nu_c}^{\infty} K_{5/3}(\eta) d\eta \text{ , erg sec}^{-1} \text{ Hz}^{-1} \quad (2)$$

where $$\nu_c = 6.27 \times 10^{18} H_{\perp} E^2 \text{ , Hz} \quad (3)$$

and $$H_{\perp} = H \sin \theta \text{ , gauss}$$

with θ the angle between the electron velocity and H. Most of the radiated energy is distributed in the frequency interval $2\nu_c > \nu > \nu_c/2$. Some values of

$$(\nu/\nu_c) \int_{\nu/\nu_c}^{\infty} K_{5/3}(\eta)\, d(\eta)$$

are given in Table 11. A plot of P_ν vs ν for monoenergetic electrons with $\nu_c = 10^4$ Hz is shown as a dashed curve in Fig. 16. Because the infrared flux density lies above the radio flux density, it is seen from Fig. 16 that the only distribution of electrons which will produce the infrared observations and not influence the radio distribution is monoenergetic electrons. When equation (2) is integrated over a continuous distribution of electrons, more radio radiation is predicted than is observed. If it is assumed that monoenergetic electrons produce the infrared radiation, then for $\nu_c \sim 10^{14}$ Hz and H~10^{-3}[8] we get E = 100 GEV. The time for such electrons to lose half of their energy is

---

[8]The magnetic field is estimated by equating the magnetic energy density $H^2/8\pi$ to the energy density of the electrons, $n_o E$, where n_o is the number density of electrons. n_o is found by equating the observed power radiated to the power expected from the synchrotron source $P = 2.37 \times 10^{-3} n_o H_{\perp}^2 E^2 V$, where V is the volume of the source. With the help of equation (3) and with $\nu_c = 10^{14}$ Hz, $V = 10^{59}$ cm^3 and $P = 10^{40}$ erg sec^{-1} the magnetic field is $H \sim 10^{-3}$ gauss.

TABLE 11

THE FUNCTION $F(\alpha) = \alpha \int_{\alpha}^{\infty} K_{5/3}(\eta) d\eta$ (41)

α	$F(\alpha)$
0.001	.213
0.01	.445
0.10	.818
1.00	.655
10.67	.0001

$$T_{1/2} = 0.0084/H_{\perp}^{2}E(GEV) = 40 \text{ years} .$$

In light of the very peculiar distribution of electron energies required and the short life time of such electrons, it is unlikely that the extended source of infrared radiation coincident with Sagittarius A is predominately the result of synchrotron radiation. The possibility that non-thermal mechanisms other than synchrotron radiation produce the infrared radiation in the dominant source can not be ruled out at present.

If the infrared radiation originates in an optically thin H II region the observed radiation is given by (39)

$$B_{\nu} = 1.71 \times 10^{-26} (M.E.) \frac{e^{-h\nu/kT}}{T^{3/2}} \left\{ \sum_{n=n_o}^{\infty} \frac{g\ II}{n^3} e^{\frac{158,000}{n^2 T}} + \frac{g\ III\ T}{316,000} \right\} \quad (4)$$

in MKS units. T is the temperature in degrees Kelvin, g II and g III are the gaunt factors, n_o is the lowest quantum level which contributes at a given frequency ν, and M.E. is the emission measure (pc cm^{-6}). From this equation with $T = 10^4$ °K the intrinsic color ratio would be $B_{\nu}(1.65)/B_{\nu}(2.2) = 0.9$ and from equation (1) the total absorption at 0.55 μ would be 20 magnitudes. When the observed 2.2 μ flux density is corrected for this total absorption, then equation (4) gives an average emission measure in a 10 pc region of about 2×10^7 pc cm^{-6}. Although this emission measure is consistent with the measured decimeter flux density, the spectral index of -0.7 in the radio region indicates that emission from an H II region cannot account for all of the observed radio radiation. Downes and Maxwell (3) estimate an emission measure of about 10^6 pc cm^{-6} which would account for only 5% of the observed

brightness at 2.2 μ.

It is, of course, possible that the observed radiation arises from a stellar population dominated by infrared stars. If the observed energy distribution is corrected for a minimum of 10 magnitudes of absorption at 0.55 μ the source of radiation must have a color temperature of 1200 K. No other stellar grouping of this nature has been observed.

It should be emphasized that all the models in this section contradict the assumption that the galactic center is similar to the nucleus of M 31.

F. The "Point" Source of Radiation

Within 10 arc sec of the position of maximum surface brightness of the dominant source there is a spike of radiation which cannot be distinguished from a point source (Fig. 5).

It is clearly of interest to establish whether or not this source is located at or near the galactic center. If the measured color ratio $B_\nu(1.65)/B_\nu(2.2)$ of 0.15 ± 0.03 is primarily a result of interstellar absorption then the agreement with the color ratio $B_\nu(1.65)/B_\nu(2.2) = 0.20 \pm 0.03$ of the surrounding extended source is indicative that the "point" source and the extended source lie approximately in the same region of space.

If the point source is between the galactic center and the Sun, the measured color ratio indicates that the radiation comes from a cool star relatively close to the Sun. An upper limit to the probability that the source is such an infrared star can be calculated from the fact

that in the California Institute of Technology infrared sky survey the density of stars in the galactic plane with a color ratio $B_\nu(1.65)/B_\nu(2.2) < 0.3$ and with a K magnitude brighter than 3 is less than 10 $ster^{-1}$ (30). If stars with these characteristics are distributed uniformly in space, the number of stars with $K < 7$ (the source has $K = 6.7$) is less than 10^4 $ster^{-1}$ in the galactic plane. Also the observations presented in Appendix B show that the surface density of point sources with a color ratio $B_\nu(1.65)/B_\nu(2.2) < 0.3$ and within a K magnitude brighter than 6.5 is about 10^4 $ster^{-1}$ in a region within one degree of the galactic center. Therefore, the probability that the unreddened foreground star would appear within the 0.3 arc min core is less than 10^{-4}. It is also of interest to note that the results given in Appendix B show that the a priori probability of finding any star with a K magnitude brighter than 6.5 within the 0.3 arc min core is less than 10^{-2}.

If this source is a dense collection of stars which have a mean energy distribution similar to that of the nucleus of M 31, then the analysis of §VIa and §VId gives a luminosity for the "point" source of 3×10^5 $L_\odot$, a mass of 7×10^5 $M_\odot$, and a density greater than 10^9 $M_\odot$ pc^{-3} within a diameter less than 0.1 pc. The collision rate would be greater than 10^{-2} yr^{-1} (33), for a rms peculiar velocity of 200 km sec^{-1} obtained from a simple application of the virial theorem. The life time of the source would be less than 10^8 years.

If the source is a single very luminous star obscured by 27 magnitudes of visual absorption, it would have an absolute magnitude at 2.2 μ $M_k = -11.0$. Intrinsically one of the most luminous stars

known at 2.2 μ is α Orionis which has $M_k \simeq -10.5$. Although population I stars like α Orionis are not known to exist in galactic nuclei, Spitzer and Saslaw (33) have suggested that stars may form at the dynamical center of the galaxy from matter dispersed during collisions. If Spitzer and Saslaw are correct, the point-like source could be a very young massive star, like α Orionis, which has formed and evolved near the dynamical center of the galaxy.

Finally, the possibility can not be discounted that the radiation emitted from the point-like source arises in non-thermal processes. In particular, the point source could be similar to, but weaker than, the sources proposed by Shklovskii (40) to exist in the nuclei of Seyfert galaxies.

Since the source would be situated in the galactic center, it would be reddened by 27 magnitudes of visual absorption. If the observations of the point source (Table 6) are corrected for this absorption, then the flux densities shown in Table 12 result. It can be seen that the flux density as a function of frequency is relatively flat.

If the source of infrared radiation is the synchrotron mechanism, then from the arguments presented in the previous section, it is apparent that the observed infrared flux density distribution must result from a large abundance of high energy electrons; however, it is shown below that unlike the situation discussed for the dominant extended source, a continuous distribution of electrons into the low energy range is possible. The types of energy distributions allowed can be obtained by integrating equation (2) over an electron energy distribution of the form $N(E) = N_o E^{-\gamma}$. When this is done a flux density distribution of the

TABLE 12

FLUX DENSITY OF THE POINT SOURCE (ii) CORRECTED FOR 27 MAGNITUDES OF VISUAL ABSORPTION

λ (μ)	Flux Density (10^{-26} W m^{-2} Hz^{-1})
1.65	16 ± 4*
2.2	19 ± 2
3.4	17 ± 3
4.8	6 ± 3

*Error in measurement only.

general form $S_\nu = S_o \nu^{-\alpha}$ results, where $\alpha = \frac{\gamma - 1}{2}$. Since the radio source Sagittarius A has a flux density at least 5 times larger than the infrared flux density of the point source, α can be as large as 0.2 and γ can be as large as 1.4 (in the Crab Nebula $\gamma = 1.6$). Further, since the angular size of the infrared source is very small, the flux density distribution may be "cut off" in the centimeter range by synchrotron self absorption (38) (such a "cut off" is observed in 3C273B (35)). This "cut off" means that α could be much larger than 0.2 and therefore γ could be larger than 1.4.

If the equations of the previous section are used then the magnetic field would be greater than 10^{-2} gauss and the infrared radiation would be produced by electrons of an energy less than 25 GEV. The lifetime of these electrons would be less than 2 years. Since there has been no change in the 2.2 μ flux density over a one year period, there would have to be a continuous source of high energy electrons.

The flux density given at 5 μ lies considerably below the other infrared fluxes; if the intrinsic 5 μ brightness of the source is this low then the flux density distribution can not be fitted by synchrotron radiation. This fact is easily seen from equation (2) (Table 11). However, a systematic error in the measurements at 5 μ or a larger amount of interstellar absorption than that given in Table 8 is possible. More measurements of the point-like source are needed at longer wavelengths to resolve the question as to the nature of the point source.

VII. SUMMARY

We have observed an extended source of infrared radiation which we believe to be at the nucleus of the galaxy. The infrared source is similar in shape and luminosity to the nucleus of M 31, and its coordinates agree with those of the dynamical center of the galaxy.

We consider the further agreement between the position and extent of the infrared source and the radio source Sagittarius A as conclusive evidence that Sagittarius A also lies at the dynamical center of the galaxy.

We believe that the infrared radiation most likely originates from stars with a mean infrared black body temperature greater than 4000 $^{\circ}$K located at the center of the galaxy. With this assumption the visual absorption to the galactic center is about 25 magnitudes and the physical properties deduced for the galactic center are similar to those observed in the nucleus of M 31.

The observed radiation is highly concentrated toward a center; the observed surface brightness decreases away from this center as $D^{-0.8}$.

The nature of the point-like source observed near the center of the dominant source is not clear. Whether it is stellar or non-thermal in nature must await further measurements, especially at longer wavelengths.

APPENDIX A

ABSOLUTE CALIBRATION OF THE INFRARED PHOTOMETER

I. Introduction

Johnson's (15, 16) infrared system of standard stars specifies only the relative flux density received from the stars. To convert these relative flux densities into absolute energy units, a calibration employing a standard energy source must be made. A direct calibration of standard stars against a standard energy source has not been attempted in the infrared; however, the flux density received from the Sun has been measured in the infrared by Minnaert (42), Peyturaux (43), and Pierce (44). By indirect measurements, the Sun can be placed on Johnson's standard star system and an absolute calibration of the system can be determined. A calibration of this type has been carried out by Johnson (45); the purpose of this appendix is to reanalyze the calculation as to its validity.

II. Apparent Solar Magnitudes

Johnson's standard system is given in terms of magnitudes defined by $M_\lambda = -2.5 \log F_\lambda + C_\lambda$ where M_λ is the magnitude at wavelength λ, F_λ is the flux density at λ and C_λ is a constant such that $M_\lambda = 0$ for an A0V star whose visual magnitude, V, equals zero. Apparent infrared solar magnitudes have not been measured on an infrared photometer, however, the apparent visual magnitude on the UBV system has been measured by several observers. The most

recent results are shown in Table 1A. We will adopt the value V = -26.74 ± .03. The infrared colors of the Sun $(V-M_\lambda)$ can be estimated from stars thought to be similar to the Sun. Kron (50) has published a list of stars whose colors in the 0.3 to 1.0 μ range are similar to the colors measured directly for the Sun. These stars also have spectral types which are similar to the Sun. Infrared measurements made on nine of these stars by Johnson, Mitchell, Iriarte and Wisniewski (16) and Johnson (45) are shown in Table 2A; the photometric magnitudes measured on our system agree with Johnson's magnitudes to within 3 percent. H, K, and L are the magnitudes (M_λ) at 1.65, 2.2, and 3.4 μ respectively. The adopted infrared colors and the standard deviations for the Sun are shown on the bottom row.

III. The Solar Energy Distribution

The mean solar flux density measured at the earth as a function of wavelength is tabulated in Allen (51). The infrared data out to 2.5 μ are taken from the work of Minnaert (42) (using the data of Abbot (52)), from Peyturaux (43), and from Pierce (44). All three authors show agreement in the range 2.0 - 2.5 μ within three percent rms. There is added evidence that the measured infrared energy distribution is correct because an extrapolation of the solar energy distribution from 1 μ out to 2 μ, using a 6000° to 5600° K black body, gives the measured answer to within ± 3%. The choice of these temperatures comes from the fact that measured brightness temperatures are $T_\odot$ = 6200° K at .6 μ and $T_\odot$ = 5200° K at 8.5 μ (53). For analysis of the energy calibration it has been assumed that the accuracy of Allen's solar energy distribution is ± 3%.

TABLE 1A

APPARENT VISUAL MAGNITUDE OF THE SUN

Observer	$V_\odot$	Error
Nikinov (46)	-26.81	± .10
Kariagina (47)	-26.83	± .09
Stebbins and Kron (48)	-26.73	± .03
Gallouet (49)	-26.70	± .02

TABLE 2A

INFRARED COLORS OF KRON'S (50) SUN-LIKE STARS

B. S.	Ref.	V	V-H*	V-K	V-L	Spectral Type
458	(16)	4. 10	1. 19	1. 25 ± . 02	1. 31 ± . 05	F8V
483	(16)	4. 96	1. 33	1. 39 ± . 03	1. 54 ± . 05	G2V
1729	(16)	4. 71	1. 35	1. 42 ± . 04		G0V
3881	(16)	5. 10	1. 33	1. 38 ± . 05		G1V
4983	(16)	4. 26	1. 30	1. 36 ± . 02	1. 49 ± . 04	G0V
5869	(16)	4. 43	1. 33	1. 39 ± . 03	1. 42 ± . 07	G0V
7504	(16)	6. 20	1. 47	1. 55 ± . 04	1. 62 ± . 04	G5V
8729	(16)	5. 50	1. 44	1. 51 ± . 03	1. 72 ± . 04	G4V
HD 157089	(45)	7. 00	1. 44	1. 46	1. 72	G0V
Sun		-26. 74 ± . 03	1. 35 ± . 07	1. 42 ± . 07	1. 53 ± . 14	G2V

*H = 0.81 K + 0. 19 J ± 0. 06 .

IV. Calculation

The following quantities have been determined by numerical integration of three of the response functions, R_λ, given in Table 2 of the text.

$$\lambda_{eff} = \frac{\int_0^\infty R_\lambda \lambda \, d\lambda}{\int_0^\infty R_\lambda \, d\lambda} \tag{1a}$$

$$\overline{F_\odot} = \frac{\int_0^\infty R_\lambda F_{\lambda\odot} \, d\lambda}{\int_0^\infty R_\lambda \, d\lambda} \tag{2a}$$

$F_{\lambda\odot}$ is the solar energy distribution discussed in section III, λ_{eff} is the effective wavelength of the band pass, and $\overline{F_\odot}$ is the average flux density received from the Sun within the bandpass. The results of integrals, the solar magnitudes, and the resultant calibration flux densities, defined as the flux density received from a star whose magnitude M_λ equals zero, are shown in Table 3A. The errors assigned to the calibration flux densities are plus or minus one standard deviation and are primarily the result of the uncertainty in the apparent magnitudes of the Sun. It should be pointed out that the relative calibration between the three bands is accurate to about ± 5%, an error considerably smaller than the one assigned to each bandpass.

V. Systematic Effects on the Calibration

The calculations of λ_{eff} and $\overline{F_\odot}$ have been carried out using a mean atmospheric transmission corresponding to about 5 mm of

TABLE 3A

SOLAR AND CALIBRATION FLUX DENSITIES

λ_{eff} (μ)	$\overline{F_{\odot}}$ (10^{-3} W cm^{-2} μ^{-1})	Solar Magnitude	Calibration Flux Density (10^{-14} W cm^{-2} μ^{-1})
1.65	19.9 ± 0.6	-28.09 ± .08	11.6 ± 1.0
2.2	7.38 ± 0.20	-28.16 ± .08	4.00 ± .35
3.4	1.61 ± 0.10	-28.27 ± .14	0.79 ± .13

precipitable water. The effects of assuming much more or less water have been evaluated using the two transmission curves of Taylor and Yates (54) which correspond to 1.4 mm and 54 mm of precipitable water. At 1.65 μ and 2.2 μ the changes in λ_{eff} and $\overline{F_{\odot}}$ are less than $\pm$ 2% even with these extreme changes in transmission. At 3.4 μ, the large absorption bands between 3.1 and 3.4 μ produce a marked effect on the bandpass characteristics, with λ_{eff} and $\overline{F_{\odot}}$ changing by as much as $\pm$ 8%. The error introduced by this change was considered when evaluating the calibration flux density.

The evaluation of λ_{eff} from equation (1a) is only valid if the flux density distribution of the object being measured is approximately flat across the wavelength band. For the galactic center observations at 1.65 μ, this is not necessarily true and a more accurate effective wavelength can be calculated from the equation

$$\lambda'_{eff} = \frac{\int_0^\infty F_\lambda^{object} R_\lambda \lambda \, d\lambda}{\int_0^\infty F_\lambda^{object} R_\lambda \, d\lambda} \qquad (3a)$$

where F_λ^{object} is the flux density distribution of the object being measured. For the galactic center data $\lambda'_{eff} = 1.68$ μ, while for the Sun $\lambda'_{eff} = 1.64$ μ. These small shifts in the effective wavelength of the measurements have been neglected.

VI. Calibration Checks

Two checks have been made on the flux calibration. The first consisted of a comparison with Strom and Avrett's (55)

atmospheric models of A0V type stars. The procedure was to find the model which best fitted Oke's (56) absolute calibration of α Lyr in the wavelength region from 0.5 to 1.1 μ, and then to use that model to determine the absolute flux density at 1.65, 2.2, and 3.4 μ. The absolute flux density at 0.54 μ was assumed to be 3.80 ± 0.05 W m^{-2} Hz^{-1} (Code (57), Johnson (45), and Willstrop (58)). Using the model $T_e = 10,000^\circ$, and $g = 4$ the calculated flux densities for a zeroth magnitude star are shown in Table 4A. Although the model atmosphere gives consistantly larger flux densities, the agreement with the adopted values is within the assigned errors.

The final check on the calibration comes from an absolute calibration made in the laboratory immediately following an observation on the 60-inch telescope. The calibration was performed on a standard black-body source. The energy emitted by the source was known to be accurate to about 10%. To obtain the absolute calibration the following assumptions were made: (a) The response of the detector was the same in the laboratory as on the telescope. (b) The average transmission of the atmosphere was 90%. (c) The reflectivity of the telescope mirrors was 95%. (d) The detector system viewed the 60-inch mirror with an efficiency of 75%. The resultant calibration flux was

$$4.6 \pm 1.0 \times 10^{-14} \text{ W cm}^{-2} \mu^{-1} .$$

Each correction factor mentioned above was assigned an error of 2/3 of the total correction. All corrections and errors were set down before performing the calculation, so that the agreement with the adopted value of $4.0 \pm 0.3 \times 10^{-14}$ W cm^{-2} μ^{-1} is significant.

TABLE 4A

CALIBRATION FLUX DENSITIES DETERMINED

FROM MODEL ATMOSPHERES

λ (μ)	Flux Model Atmosphere (10^{-14} W cm^{-2} μ^{-1})	Flux Adopted (Table 3A) (10^{-14} W cm^{-2} μ^{-1})
1.65	12.6	11.6 ± 1.0
2.2	4.45	4.00 ± 0.35
3.4	0.83	0.79 ± 0.13

VII Adopted Calibration

The adopted calibration flux densities for each of the five wavelength bands used to observe the galactic center are shown in Table 5A; by definition the calibration flux density is the flux density received at the top of the atmosphere of the earth from a zeroth magnitude star. At 1.65, 2.2 and 3.4 μ the results of section IV are given, while at 4.8 and 0.85 μ, where very few observations were made, the results of Johnson (45) are shown. The 4.8 μ calibration of Johnson has an uncertainty of at least 20% because 4.8 μ magnitudes of solar-type stars have not been measured.

TABLE 5A

ADOPTED FLUX DENSITY OF A ZEROTH MAGNITUDE STAR

λ_{eff}	Adopted Calibration		Johnson's Calibration (45)
(μ)	F_λ (10^{-14} x W cm^{-2} μ^{-1})	F_ν (10^{-24} x W m^{-2} Hz^{-1})	F_λ (10^{-14} x W cm^{-2} μ^{-1})
0.85	8.3 ± .8	22.4 ± 2.0	8.3
1.65	11.6 ± 1.0	10.5 ± 1.0	
2.2	4.0 ± .3	6.5 ± 0.5	3.9
3.4	0.79 ± .1	3.0 ± 0.4	0.81
4.8	0.22 ± .05	1.8 ± 0.4	0.22

APPENDIX B

FURTHER 60-INCH OBSERVATIONS OF THE GALACTIC CENTER REGION DURING 1967

I. Introduction

During May and July, 1967 further infrared photometric observations were made of the galactic center region using the 60-inch telescope at Mt. Wilson. These new observations were made for the following reasons: (a) to determine the uniqueness of the dominant source of radiation coincident with Sagittarius A (section V a(i)), (b) to better determine the colors of the dominant and secondary extended sources, and (c) to determine the colors and surface number densities of the unresolved point-like sources in the region of the galactic center. Although the observations were made under poor observing conditions, information concerning the problems mentioned above was obtained. The results of these observations are presented in this Appendix.

II. Observations

The observations were made using the same photometer described in the text. Simultaneous measurements were taken at 2.2 μ and at either 0.85 or 1.65 μ; both systems had a 0.8 arc min diameter field of view and a reference beam 7 arc min east of the signal beam. During the observations the telescope was kept fixed with respect to the earth and the sky drifted by at sidereal rate; therefore, an object passed first through the reference beam of each system producing a negative signal and then through the signal beam producing a positive

signal. The scans were positioned so that they lay approximately across the galactic plane. A summary of the observations made on 25 May and 10 and 11 July 1967 are shown in Table 1B; the total area covered was several square degrees.

The position of the scans in the sky, the energy response of the detectors, and the surface response of the detector systems were all determined by observing Johnson's (16) standard stars in exactly the same way as the galactic center.

III. Data

From the strip chart tracings of the RA scans, summarized in Table 1B, all the sources of radiation brighter than a given flux level were listed. The sources found were divided into two groups: (a) objects which were unresolved and appeared point-like, (b) objects which were resolved into extended sources of radiation. To make the sample of point-like sources as free as possible from selection effects, only sources which had a 2.2 μ signal to noise larger than 5 and which had a scan width larger than 70% of the aperture diameter were chosen. The latter restriction meant that the effective width of the scan patterns for detecting point sources was about 0.55 ± 0.10 arc min.

The observed point-like sources are a representative sample of all the sources present which have a 2.2 μ flux density larger than 1.6×10^{-26} W m^{-2} Hz^{-1} (K = 6.5 mag). Table 2B lists all of the point-like sources found on 27 May 1967 and Table 3B lists the sources found on 10 and 11 July 1967; the tables include the flux density, position in the sky, and color ratio $S_\nu(0.85)/S_\nu(2.2)$ or $S_\nu(1.65)/S_\nu(2.2)$ of each

TABLE 1B

RECORD OF OBSERVATIONS

Date	λ (μ)	No. of Scans	Length of Scans (arc min)	Declination Region Covered	Separation of Each Scan (arc min)
27 May 1967	2.2, 0.85	10	250	-28°57' to -28°06'	1
10 July 1967	2.2, 1.65	21	100	-28°48' to -29°08'	1
11 July 1967	2.2, 1.65	47*	50	-27°59' to -28°49' -29°09' to -29°49'	2

*For five of these scans there were clouds which reduced the sensitivity by about a factor of 2.

TABLE 2B

POINT-LIKE SOURCES FOUND ON 27 MAY 1967

Dec. (1950)	RA(1950)	$S_\nu(2.2)$ (10^{-26} W m^{-2} Hz^{-1})	$S_\nu(0.85)/S_\nu(2.2)$	$S_\nu(1.65)/S_\nu(2.2)$*
	h m s			
-28°57'	17 35 40	3.4	0.2	
-28°58'	17 34 10	4.5	< 0.1	
	17 40 17	2.6	< 0.1	
	17 46 55	1.9	0.6	
-28°59'	17 38 17	1.7	< 0.2	
	17 39 55	2.5	0.2	
	17 42 55	1.6	0.2	
-29°01'	17 41 20	2.8	< 0.1	
	17 42 57	3.0	0.4	
-29°02'	17 33 48	2.0	< 0.2	1.1
	17 43 40	> 8.0		
	17 44 18	6.2	0.15	
	17 48 10	3.4	< 0.1	
-29°03'	17 38 48	1.9	< 0.2	
	17 42 15	1.6	< 0.2	
	17 43 21	3.3	< 0.1	
	17 44 35	> 8.0	< 0.02	0.4
	17 45 48	1.6	0.9	
	17 49 40	5.1	0.7	
	17 50 33	3.2	< 0.1	0.9
	17 51 47	5.4	0.1	
-29°04'	17 33 33	4.3	0.1	
	17 42 53	3.7	0.5	
	17 45 21	4.9	0.3	
	17 46 05	> 8.0	< 0.3	
	17 50 45	1.6	< 0.2	
-29°05'	17 38 01	2.0	< 0.2	0.7
	17 45 55	2.3	< 0.2	
-29°06'	17 39 45	1.6	< 0.2	
	17 42 07	2.5	< 0.2	0.4
	17 43 48	2.2	< 0.2	0.5
	17 43 56	2.5	< 0.2	1.0
	17 44 18	2.3	0.8	1.7

*Data obtained on 29 May 1967.

TABLE 3B

POINT-LIKE SOURCES FOUND ON 10 AND 11 JULY 1967

Date	Dec. (1950)	RA(1950)	$S_\nu(2.2)$ (10^{-26} W m^{-2} Hz^{-1})	$S_\nu(1.65)/S_\nu(2.2)^+$
10 July	-28°48'	$17^h\ 41^m\ 21^s$	1.9	0.5
		17 44 43	2.5	0.7
	-28°49'	17 42 42	1.9	1.0
	-28°51'	17 38 22	2.5	1.0
		17 40 21	7.5	0.8
		17 41 52	2.3	1.4
	-28°53'	17 37 50	3.8	1.6
	-28°54'	17 42 54	1.9	1.1
		17 45 32	4.2	0.9
	-28°56'	17 40 22	2.9	0.5
		17 45 49	2.9	1.2
	-28°57'	17 39 55	1.9	0.6
		17 40 45	4.0	1.3
		17 42 57	2.7	0.5
		17 43 03	2.3	1.3
	-28°58'	17 44 33	2.1	0.9
		17 44 41	3.4	0.8
	-29°00'	17 45 31	1.6	1.3
	-29°01'	17 42 57	5.0	1.2
	-29°02	17 43 41	34.0	
		17 44 22	4.4	1.2
	-29°03'	17 38 47	2.1	0.8
		17 42 44	3.5	0.5
		17 43 20	6.1	0.7
		17 44 34	28.0	0.4
	-29°04'	17 42 53	5.5	1.3
		17 42 56	1.2	1.5
		17 45 21	5.5	1.2
	-29°05'	17 37 57	4.2	0.4
	-29°06'	17 39 39	2.7	0.6
		17 41 32	3.2	0.4
		17 43 42	3.0	0.7
		17 43 50	2.3	1.4
		17 44 15	3.6	1.5
	-29°07'	17 38 35	5.0	0.8
		17 38 51	1.7	0.7
		17 39 51	7.5	0.6
	-29°08'	17 40 49	1.6	0.5
		17 42 04	2.5	1.6

TABLE 3B--Continued

Date	Dec. (1950)	RA(1950)	$S_\nu(2.2)$ (10^{-26} W m^{-2} Hz^{-1})	$S_\nu(1.65)/S_\nu(2.2)$+
11 July	-28°05'	17h 43m 19s	24.0	
	-28°09'	17 44 04	3.4	1.1
	-28°11'	17 44 22	1.7	0.6
		17 46 43	2.5	1.8
	-28°13'	17 43 09	1.7	0.7
		17 43 13	2.5	1.0
		17 43 44	2.1	0.5
		17 44 23	1.7	0.5
	-28°17'	17 45 11	1.7	< 0.4
	-28°19'	17 45 30	4.2	1.3
	-28°25'	17 45 09	1.6	0.9
	-28°27'	17 43 19	2.5	1.2
	-28°31'	17 42 32	2.1	< 0.4
	-28°35'	17 42 37	3.4	0.5
		17 42 42	4.2	0.6
		17 42 47	14.0	1.0
		17 43 57	31.0	
		17 45 17	3.4	1.3
	-28°37'	17 42 01	4.2	0.5
		17 42 39	1.7	0.7
	-28°41'	17 41 58	1.7	0.6
		17 44 27	3.4	1.2
	-29°11'	17 44 52	3.4	1.0
	-29°13'	17 41 08	5.0	1.4
	-29°15'	17 41 14	4.6	0.9
		17 44 19	4.7	1.1
	-29°19'	17 43 42	3.4	1.4
	-29°23'	17 43 42	27.0	
	-29°27'	17 39 52	3.8	0.7
		17 43 42	8.4	1.5
	-29°31'	17 43 08	5.9	0.7
	-29°33'	17 41 48	4.2	1.0
	-29°41'	17 41 12	2.1	< 0.3
		17 43 32	13.0	1.0
	-29°45'	17 40 11	2.1	0.5
	-29°47'	17 40 12	1.7	< 0.5
	-29°49'	17 41 11	5.9	1.3

+The ratio for an A0V stars is 1.6 .

source found. From regions of the sky where there was an overlapping of data, the errors in the flux density and color are estimated to be 20 and 30% respectively. The distribution in galactic coordinates of point-like sources found on 10 and 11 July 1967 at odd minute declinations is shown in Fig. 1B. It should be emphasized that the survey was not spatially complete and thus gives only a sample of the sources present.

Table 4B shows a summary of the extended sources found with a maximum 2.2 μ surface brightness of 2×10^{-19} W m^{-2} Hz^{-1} $ster^{-1}$ over an area 0.8 arc min in diameter. Sources with similar right ascensions in adjacent declineation scans have been grouped together. The approximate extent of each source in right ascension and the color ratio $B_\nu(1.65)/B_\nu(2.2)$ are also given. The error in the maximum surface brightness is generally about $\pm 2 \times 10^{-19}$ W m^{-2} Hz^{-1} $ster^{-1}$; the error in the color ratio for all sources other than the dominant source is about $\pm 50\%$. For the central part of the dominant source the error in color is about $\pm$ 20%. Table 4B is not complete, since the 7 arc min separation of the two beams discriminates both against sources with diameters larger than 7 arc min and against faint sources within 7 arc min of a stronger source.

IV. Discussion of Data

a) Extended Sources of Radiation.

From the data presented in the previous section, the following statements can be made concerning the extended sources of radiation.

Figure 1B

Surface distribution of point-like sources in the galactic center region. Shown are sources with a 2.2 μ flux density larger than 1.6×10^{-26} W m^{-2} Hz^{-1} that were found with an 0.8 arc min aperture while scanning in delination intervals of 2 arc min. (The effective width of the aperture for detecting sources was about 0.55 arc min.)

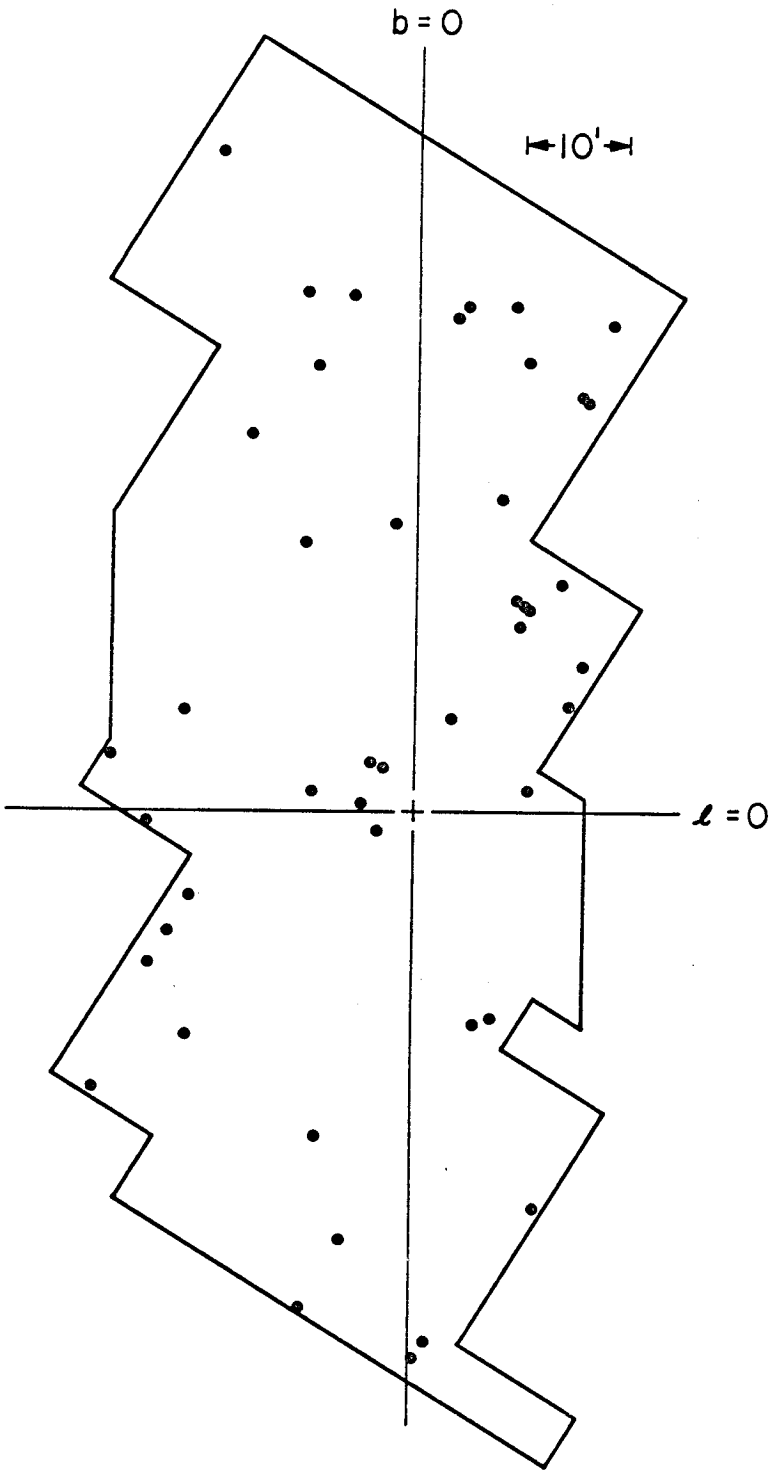

Figure 1B

TABLE 4B

EXTENDED SOURCES FOUND ON 10 AND 11 JULY 1967

Source*	Dec. (1950)	RA (1950)	ΔRA (arc min)	$B_\nu^{max}(2.2)$ (10^{-19} x W m^{-2} Hz^{-1} $ster^{-1}$)	$B_\nu(1.65)/B_\nu(2.2)$
		h m s			
Dominant	-28°50'	17 43 04	6	2	.50
	-28°51'	17 42 54	10	2	.70
	-28°53'	17 42 59	6	2	.35
	-28°54'	17 43 04	6	3	.35
	-28°55'	17 42 54	6	3	.30
	-28°56'	17 42 44	4	6	.35
	-28°57'	17 42 44	2	13	.35
	-28°58'	17 42 42	2	25	.20
	-28°59'	17 42 34	2	34	.20
	-29°00'	17 42 37	2	17	.25
	-29°01'	17 42 34	6	6	.20
	-29°02'	17 42 24	6	5	.30
	-29°03'	17 42 24	6	6	--
	-29°04'	17 42 14	6	8	.30
	-29°05'	17 42 14	4	5	.20
	-29°06'	17 42 14	6	4	.35
	-29°07'	17 42 14	6	3	.45
	-29°08'	17 42 14	9	4	.35
	-29°11'	17 42 14	4	4	.30
	-29°15'	17 41 59	2	4	.55

TABLE 4B--Continued

Source*	Dec. (1950)	RA (1950)	ΔRA (arc min)	$B_\nu^{max}(2.2)$ (10^{-19} x W m^{-2} Hz^{-1} $ster^{-1}$)	$B_\nu(1.65)/B_\nu(2.2)$
		h m s			
B	-28°55'	17 44 34	6	3	.40
	-28°56'	17 44 34	4	2	.55
	-28°57'	17 44 34	6	4	--
	-29°58'	17 44 39	6	4	.70
	-28°59'	17 44 19	4	3	.65
	-29°00'	17 44 24	8	4	.70
	-29°01'	17 44 09	6	4	.70
	-29°02'	17 44 24	8	4	--
	-29°03'	17 44 14	9	4	--
E	-28°59'	17 43 04	6	3	.20
	-29°00'	17 43 09	6	3	.40
G	-29°07'	17 41 14	3	4	.70
	-29°08'	17 41 29	3	4	.75
	-29°09'	17 41 14	3	4	1.00
	-28°51'	17 41 14	6	2	.80
	-28°53'	17 41 14	6	2	.25
	-28°54'	17 41 14	6	2	.30
	-29°09'	17 42 59	6	4	.55
	-29°11'	17 43 04	4	6	.70
	-29°37'	17 42 24	10	2	.70

*Refer to Table 7 of the text.

1) There is no other extended source of radiation similar to the dominant source within an area 7×10^3 square arc min (2 square degrees) surrounding the galactic center.
2) The surface number density of extended sources decreases sharply as one goes away from the galactic center.
3) The average color of the extended sources is bluer than the dominant source, but redder than the point-like sources.

The uniqueness of the dominant source can be seen by comparing the characteristics of the dominant source with those of the other sources found. The dominant source of radiation has a surface brightness which increases rapidly towards the center with a maximum value of 3.5×10^{-18} W m^{-2} Hz^{-1} $ster^{-1}$ at 2.2 μ over an 0.8 arc min diameter area, it has a total 2.2 μ flux density larger than 3×10^{-24} W m^{-2} Hz^{-1}, and it has a color ratio $B_\nu(1.65)/B_\nu(2.2) = 0.2$. All of the secondary sources found in Table 4B and in Fig. 5 of the text have a maximum 2.2 μ surface brightness of less than 0.6×10^{-18} W m^{-2} Hz^{-1} $ster^{-1}$ over an 0.8 arc min diameter area. The strongest secondary source is B which has a total flux density less than 2×10^{-24} W m^{-2} Hz^{-1}. All of the secondary sources measured, except source E, have a color ratio $B_\nu(1.65)/B_\nu(2.2)$ two to four times larger than the dominant source. In summary, of all the extended sources measured, the dominant source has the highest surface brightness, the largest flux density and the reddest color.

The positional variation of the surface number density of the extended sources is seen from the data in Table 4B. The surface density of the extended sources is larger than 10^{-2} per sq. arc min in a region

30 arc min in diameter centered on the dominant source, whereas the surface density of sources in the region 15 to 50 arc min from the galactic center is less than 10^{-3} per square arc min.

The colors of the extended sources are also shown in Table 4B. The average color ratio $B_\nu(1.65)/B_\nu(2.2)$ is about 0.6, which is considerably larger than the value 0.2 measured for the dominant source. This result agrees with the data discussed in section V a(iv) of the text; thus the conclusions reached there are still valid.

It is interesting to note that the color of the dominant source appears to become bluer as the distance from the center of the source is increased. Since the effect is seen along the galactic plane, it is unlikely that the color change can be a result of foreground reddening (section V a(iv) of the text). There are at least three other possible explanations: (a) the intrinsic color of the source changes as a function of radial distance from the center of the source, (b) a considerable amount of interstellar absorption ($A_V \sim 10$) exists within 50 pc of the galactic center, and, (c) the two beam photometer produces a systematic mistake in the color measurements. Further data are needed to resolve this question.

b) Point-like Sources of Radiation.

The unresolved point-like sources of radiation have at least three apparent properties.

1) The surface density of sources with a flux density larger than 1.6×10^{-26} W m^{-2} Hz^{-1} near the galactic center is $3.0 \pm 1.0 \times 10^{-2}$ per square arc min.

2) The surface number density of the sources appears to be uniform over the entire region measured (~ 2 square degrees).

3) The mean color ratio $B_\nu(1.65)/B_\nu(2.2)$ of the sources is about 0.9, which is slightly redder than an average K or M star which has a color ratio from 1.2 to 1.4.

The mean calculated surface number density of sources is similar to the density expected from extrapolation of the results of the infrared sky survey. Hughes (30) has shown that the density of sources within the region $|b^{II}| < 2°$, $0 < \ell^{II} < 90°$ with a flux density larger than 36×10^{-26} W m^{-2} Hz^{-1} is 2.5×10^{-4} per square arc min. Assuming a uniform spacial density of sources, one would expect 2.5×10^{-2} source per square arc min with a flux density greater than 1.6×10^{-26} W m^{-2} Hz^{-1}. The slight excess in the measured source density may indicate the presence of a density gradient towards the galactic center. Using Schmidt's (59) calculated mass density gradient $d \log \rho / d\tilde{\omega} = 0.18$ as an upper limit to the gradient of infrared stars it can be concluded that the 1.6×10^{-26} W m^{-2} Hz^{-1} sources are within 2 or 3 kpc of the Sun.

How uniformly distributed the point-like sources appear in the sky can be seen in Fig. 1A and in Tables 5B and 6B, where the density of sources is given as a function of ℓ and b. The size of the regions for which data are given in Table 5B is about 60 arc min long in b and 20 arc min wide in ℓ, while the size of the regions in Table 6B is about 120 arc min long in ℓ and 10 arc min wide in b. There appears to be a slight tendency for the surface number density of sources to increase towards the center as a function of ℓ; however, the densities found are

TABLE 5B

SURFACE NUMBER DENSITY OF POINT-LIKE SOURCES AS A FUNCTION OF ℓ

Region	$\bar{\ell}$ (arc min)	No. of Stars	Region Scanned* (sq. arc min)	Density (sq. arc min)$^{-1}$
1	60	7	1000	$2.6 \pm 1.0 \times 10^{-2}$
2	40	7	900	2.8 ± 1.0
3	20	10	1000	3.6 ± 1.0
4	0	9	900	3.6 ± 1.2
5	-20	6	950	2.4 ± 1.0
6	-40	6	1000	2.2 ± 1.0

*The true area scanned is about 1/3 this value.

TABLE 6B

SURFACE NUMBER DENSITY OF POINT-LIKE SOURCES AS A FUNCTION OF b

Region	$\bar{b}$ (arc min)	No. of Stars	Region Scanned* (sq. arc min)	Density (sq. arc min)$^{-1}$
1	+10	11	1200	$3.3 \pm 1.0 \times 10^{-2}$
2	0	9	1300	2.5 ± 1.0
3	-10	9	1300	2.5 ± 1.0
4	-20	6	1200	1.8 ± 1.0

*The true area scanned is about 1/3 this value.

very consistant with a random distribution. (The χ^2 of the ℓ regions assuming a random distribution of sources is 2.0; a χ^2 larger than this occurs 80% of the time.) From the data of 10 July 1967 it is found that the density of sources with $20 < |b| < 60$ arc min is $2.9 \pm 0.6 \times 10^{-2}$ per square arc min which is in agreement with the data in Table 6B for $|b| < 20$ arc min.

The mean color ratio $B_\nu(1.65)/B_\nu(2.2)$ of the point-like sources is about 0.9 with an rms spread of about $\pm$ 0.4; the average color ratio is also about 0.9. This color ratio is somewhat smaller than that expected from the results of the infrared sky survey, where the mean color $B_\nu(1.65)/B_\nu(2.2)$ of the sources found is inferred to be approximately 1.2 from the mean measured color $B_\nu(0.75)/B_\nu(2.2)$. The difference between the galactic center region and the sky survey results could be explained by approximately 4 magnitudes of visual absorption. The color ratio $B_\nu(0.85)/B_\nu(2.2)$ measured in the galactic center region is also consistant with approximately 4 magnitudes of visual absorption.

It is of interest to determine from these data the surface number density of sources similar to the point source discussed in section VI f of the text. Taking the data of 10 and 11 July 1967, only four sources have a color ratio $B_\nu(1.65)/B_\nu(2.2) < 0.3$, therefore the surface number density of such sources with a K magnitude brighter than 6.5 is less than 2×10^4 ster^{-1}.

In summary it is clear that the point-like sources are not spacially located at the galactic center since they have a surface density which is only slightly larger than that found in the local

neighborhood from the infrared sky survey, they show no marked tendency to occur predominately in the immediate vicinity of the galactic center, and they show a mean absorption which is only 15% of the absorption to the galactic center.

It appears that the unresolved point-like sources are of the same nature as the sources found on the infrared sky survey; the exact characteristics of these objects is still unknown, but a majority are probably K and M giant stars (30).

REFERENCES

1. Oort, J. H., and Rougoor, G. W., M. N., 121, 171 (1960).
2. I. A. U. Bulletin, No. 11, p. 11, (1963).
3. Downes, D., and Maxwell, A., Ap. J., 146, 653 (1966).
4. Stebbins, J., and Whitford, A. E., Ap. J., 106, 235 (1947).
5. Baade, W., Pub. of the Obs. of the Univ. of Mich., 10, 7 (1951).
6. Dufay, J., Ann. Astrophys., 23, 451 (1960).
7. Arp. H., Ap. J., 141, 43 (1965).
8. Baade, W., Mitt. Astr. Ges., 51 (1955).
9. Hubble, E., Ap. J., 69, 103 (1929).
10. Lallemand, A., Duschesne, M., and Walker, M. F., Pub. A.S.P., 72, 76 (1960).
11. Moroz, V. I., Soviet Astronomy - A. J., 5, 361 (1961).
12. Whitford, A. E., A. J., 63, 201 (1958).
13. Johnson, H. L., and Morgan, W. W., Ap. J., 117, 313 (1953).
14. Westphal, J. A., Murray, B. C., and Martz, D. E., Appl. Opt., 2, 749 (1963).
15. Johnson, H. L., Bol. Ton. Y. Tac. Obs., 3, 305 (1964).
16. Johnson, H. L., Mitchell, R. I., Iriarte, B., and Wisniewski, W. Z., Comm. Lunar and Planet. Lab., 4, 99 (1966).
17. Hughes, E. E., Private Communication (1965).
18. Downes, D., Maxwell, A., and Meeks, M. L., Nature, 208, 1189 (1965).
19. Neugebauer, G., and Becklin, E., to be published (1968).
20. Sandage, A., Ap. J., 127, 513 (1958).
21. Johnson, H. L., Ap. J., 143, 187 (1966).

22. Johnson, H. L., and Borgman, J., B. A. N., 17, 115 (1963).

23. Johnson, H. L., Ap. J., 141, 923 (1965).

24. Hulst, H. C., van de, Rech. Astro, Obs. Utrech., 11, Part 2 (1949).

25. Rougoor, G. W., and Oort, J. H., Proc. N. A. S., 46, 1 (1960).

26. Kinman, T. D., Ap. J., 142, 1376 (1965).

27. Pooley, G. G., Kenderdine, S., Nature, 214, 1190 (1967).

28. Neckel, T., Z. Astrophys., 63, 221 (1966).

29. Johnson, H. L., Stars and Stellar Systems, Vol. VII: Nebulae and Interstellar Matter, ed. L. H. Aller and B. M. Middlehurst, (Chicago: University of Chicago Press) (1967).

30. Hughes, E. E., Private Communication (1967).

31. Schmidt, M., B. A. N., 14, 17 (1957).

32. Spinrad, H., Ap. J., 135, 715 (1962).

33. Spitzer, L., and Saslaw, W. C., Ap. J., 143, 400 (1966).

34. Epstein, E., Private Communication (1967).

35. Howard, W. E., and Maran, S. P., Ap. J. Supp., 10, 1 (1965).

36. Pacholczyk, A. G., and Wisniewski, W. A., Ap. J., 147, 394 (1967).

37. Low, F. J., and Johnson, H. L., Ap. J., 141, 336 (1965).

38. Slysh, V. I., Nature, 199, 628 (1963).

39. Moroz, V. I., Soviet Astr. - A. J., 7, 601 (1964).

40. Shklovskii, I. S., Soviet Astr. - A. J., 9, 683 (1966).

41. Oort, J. H., and Walraven, T., B. A. N., 12, 285 (1956).

42. Minnaert, M., B. A. N., 2, 75 (1924).

43. Peyturaux, R., Ann. Astrophys., 15, 302 (1952).

44. Pierce, A. K., Ap. J., 119, 312 (1954).

45. Johnson, H. L., Comm. Lunar and Plant. Lab., 3, No. 53 (1965).

46. Nikinov, E. K., Izvest. Crimean Astr. Obs., 4, 114 (1949).

47. Kariagina, S. W., Izvest. Astr. Inst. Alma-Ata., 1, 85 (1955).

48. Stebbins, J., and Kron, G. E., Ap. J., 126, 266 (1957).

49. Gallouet, L., Ann. Astrophys., 27, 423 (1964).

50. Kron, G. E., Pub. A.S.P., 75, 288 (1963).

51. Allen, C. W., Astrophysical Quantities (London: Athlone Press), (1963).

52. Abbot, C. G., Ann. Ap. Ob. Smith Ins. IV, 192 (1922).

53. Saiedy, F., M. N., 121, 483 (1960).

54. Taylor, J. H., and Yates, H. W., J. of Opt. Soc. of Am., 47 223 (1956).

55. Strom, S. E., and Avrett, E. H., Ap. J. Suppl. 12, 1 (1965).

56. Oke, J. B., Ap. J., 140, 689 (1964).

57. Code, A. D., Stars and Stellar Systems, Vol. VI: Stellar Atmospheres, ed. J. L. Greenstein (Chicago: University of Chicago Press) (1960).

58. Willstrop, R. V., M. N., 121, 17 (1960).

59. Schmidt, M., Stars and Stellar Systems, Vol. V: Galactic Structure, ed. A. Blaauw and M. Schmidt (Chicago: University of Chicago Press) (1965).